Chapter 6

Stress Induced Changes in the Raman Spectrum of Carbon Nanostructures and their Composites

By A. S. Paipetis

Dept. of Materials Science & Engineering, University of Ioannina, Ioannina, Greece

Abstract

Raman spectroscopy of Carbon nanostructures is fundamental in characterising the morphology and the interaction of the nanostructure with the environment. This work provides an outline of the Raman Vibrational modes for graphitic structures starting from graphite fibres, to single-wall carbon nanotubes to multiwall carbon nanotubes and finally to Single- and Multi-layer Graphene. Following a brief outline of the dependence of the force constant on applied deformation, the stress induced changes in the Raman spectrum of graphitic structures are subsequently discussed with a view to elucidating the reinforcing ability of the CNTs in a matrix and assessing the stress transfer at the CNT matrix interface. The possibilities of employing CNTs as stress sensors in composite materials are also presented.

Keywords: Carbon Nanotubes, Raman Spectroscopy, stress monitoring, nanocomposites

Table of contents

Reference: Paipetis A. S. (2012). Stress Induced Changes in the Raman Spectrum of Carbon Nanostructures and their Composites. In “Carbon nanotube enhanced Aerospace Composite Materials”, A.S. Paipetis and V. Kostopoulos (eds), Springer.

6.1. Introduction

The scope of this work is to provide an overview of the stress-induced changes in the Raman spectrum of graphitic structures. As there has been limited work done in the field of hybrid composite systems, this chapter will focus on aspects related to the ability of employing the Raman technique for monitoring systems that are comprised of graphitic carbon nanostructures and their composites. This will be performed in order to provide an insight into the capabilities of the methodology as a means of sensing internal stresses and assessing the stress transfer in nano-reinforced composites.

Raman spectroscopy has always been an invaluable tool for evaluating the structure and properties of graphitic materials. Since the reference work by Tuinstra and Koenig on graphite fibres (Tuinstra,Koenig 1970), there is an immense volume of research effort that focuses on the interpretation of the Raman spectrum of sp^2 carbon allotropes. This research interest has been further boosted due to the study of fullerenes (Kuzmany et al. 2004), carbon nanotubes (CNTs) (Dresselhaus et al. 2005), and recently graphene (Malard et al. 2009b). These graphitic structures are extremely promising in that they offer exceptional mechanical, thermal and electronic properties. It is noteworthy that the in-plane elastic modulus of graphene is regarded to be the highest of all known materials, on the order of 1 TPa (Sengupta et al. 2011). The Raman spectrum of graphite provides direct information on the C-C bond which exhibits this extraordinary stiffness; note that the E_{2g} in plane vibration is the only allowable Raman Vibrational mode in graphite. In this respect, the importance of Raman monitoring of sp^2 carbon is by definition justified. All deviations from the planar hexagonal array of the infinite graphitic sheet or graphene directly affect all the aforementioned properties but at the same time give rise to other modes in a Raman spectrum (Malard et al. 2009b). This further enhances the capability of Raman Spectroscopy to monitor the sp^2 morphology, as well as the effect that any external field is expected to have on it.

The tubular morphology of single wall CNTs (SWCNTs) is of particular interest since all these “carbon molecules” may possess unique spectral signatures depending particularly on their diameter and chirality (Dresselhaus et al. 2010). These spectral

features distinguish them from the typical spectrum of carbon fibres and allow for their identification. Of particular interest are the resonance effects which are related to the dispersive nature of vibrational modes such as the Radial Breathing Mode (RBM), which are also significantly affected by the deformation that an external field may induce to the SWCNT (Dresselhaus et al. 2007). The lifting of degeneracy of the E_{2g} band in the axial and circumferential direction also leads to an alteration of the typical graphitic lines. The unique structure of double wall CNTs (DWCNTs) is mirrored in their Raman spectrum and is directly related to phenomena such as interlayer interaction and interlayer stress transfer. The Raman spectrum of multiwall CNTs (MWCNTs) is closer to the Raman Spectrum of graphite fibres, but still direct information about the stress transfer efficiency of MWCNT reinforced composites may be derived. Finally, the simplicity of graphene is unique in providing insight into all vibrational modes including the so called "disorder induced" Raman vibrational modes as well as elucidating the interlayer interaction I multi-layer graphene.

Due to the anharmonicity of the C-C bond (Wool 1980), the applied stress on all aforementioned structures is directly related to shifts in vibrational frequencies or changes in the intensities due to resonance phenomena. Splitting of bands like the graphitic (G) or the second-order graphitic (G') line is also observed (Frank et al. 2011a). The calibration of stress-induced shifts with applied strain provides direct information about the stress transfer. The derived stress dependence of Raman bands in the ideal case of Graphene may also directly link the translation of far-field stress to the C-C bond stretching, which is in fact the essence of reinforcement for nano-reinforced materials (Frank et al. 2011b). In this respect, Raman Spectroscopy is unique in providing directly stress information. In addition, the capability of employing graphitic structures as stress sensors within structural composites is also significant (Zhao et al. 2002), since the Raman Spectrum of CNTs may provide information on interfacial stress transfer (Sureeyatanapas et al. 2010) even stress concentrations around notches (Zhao,Wagner 2003).

Summarizing, Raman Spectroscopy is an invaluable tool in characterizing sp^2 graphitic structures and their composites. On the other hand, the outburst of research activity in these graphitic structures has immensely increased the research in the field of Raman spectroscopy of such materials and, as a result, the capabilities of Raman spectroscopy for stress monitoring and sensing in sp^2 structures seem to ever increase as the volume of related research is rising.

6.2. The Raman Spectrum of Graphitic Structures

Common to all graphitic structures is the Graphitic or G band which corresponds to the in-plane lattice vibrations of the plane graphitic crystal (Vidano et al. 1981). The aforementioned band is one of the two Raman active E_{2g} vibrational modes for graphite together with the band observed at approximately 50 cm^{-1} which corresponds to a rigid layer shearing of the graphitic lattice (Nemanich et al. 1977). All deviations from planar geometry and symmetry result in alterations in the G band. As a result, the G band can be used to probe any divergence from the flat geometric structure of graphene. These divergences may comprise the strain induced by external forces, by layer interaction in a graphene with few layers or in multi-wall nanotubes, or even by the curvature of the side wall in tubular structures. In the latter case, more Raman active modes are present, characterizing the diameter, the chirality rendering thus the Raman signature of every tubular geometry almost unique (Dresselhaus et al. 2010). However, the overlapping tubular geometry of multi-wall CNTs makes these spectral features less distinguishable (Malard et al. 2009b). The strong feature at approximately 2700 cm^{-1} is also characteristic of sp^2 carbon, and is characterized by its dispersive properties, or by its dependence on excitation frequency. The so-called G'-band is a second-order double resonance process and as such is very sensitive to the morphology of the structure providing information on the number of concentric tubes for multiwall nanotubes (Malard et al. 2009b). The origin of this second order feature has been greatly argued, but for reasons of consistency it will be referred to in this work as the "G' band". Interestingly enough, with an increase in the number of walls of the CNTs or equivalently with an increase in the number of layers, more double resonance scattering processes occur, and the final spectral feature converges to that of graphite, where only two peaks are observed.

Apart from the graphitic lines of the Raman Spectrum, the presence of the "disorder induced" lines is evident in most sp^2 morphologies. These two lines are observed in the first order spectrum in the vicinity of 1360 cm^{-1} and 1620 cm^{-1} and are denoted as the D and the D' line respectively (Lespade et al. 1984). The disorder induced lines are strongly interrelated and have been directly associated with experimentally induced disorder in the graphene layers or the average defect distance (Lucchese et al.

2010) as well as the graphitization temperature which is directly related to stiffness (Huang,Young 1995) or crystallite size. In the case of high modulus carbon fibres, the disorder induced bands are reported to vary along the fibre length for an individual fibre (Paipetis,Galiotis 1996) or even along the fibre cross section (Katagiri et al. 1988). The work on carbon fibres strongly suggests that apart from the amount of crystal boundary that is inversely proportional to crystal size as suggested in early works (Tuinstra,Koenig 1970), lattice orientation is also responsible for the presence or not of the disorder lines. Moreover, the chirality of the nanotubes may enhance or diminish the disorder lines in the case of armchair nanotube morphology and zigzag nanotube morphology, respectively (Cançado et al. 2004).

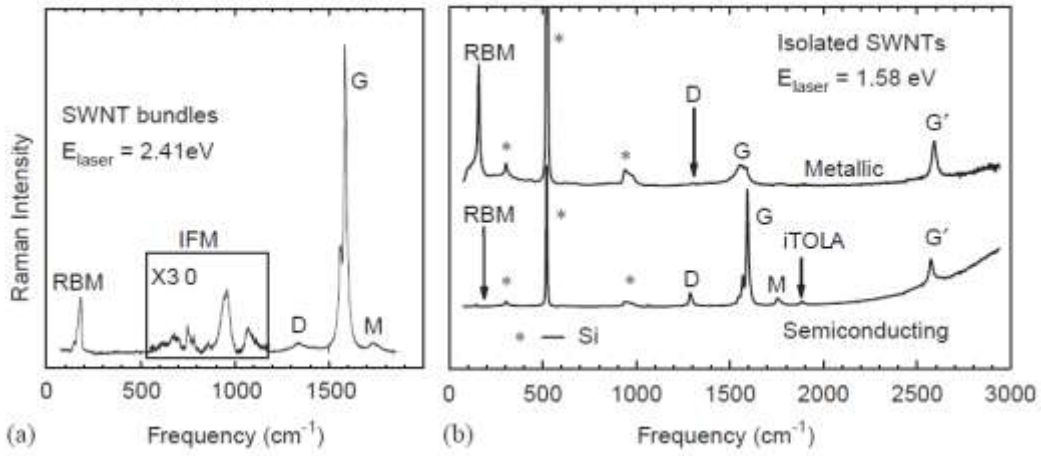

Figure 1: (a) Raman spectra from SWNT bundles (b) Raman spectra from a metallic (top) and a semiconducting (bottom) SWNT at the single nanotube level (Reprinted from (Dresselhaus et al. 2005), with permission from Elsevier)

SWCNTs are specially challenging in that their diameter is by definition smaller than that of the typical excitation wavelength. The typical Raman spectrum of SWCNTs is depicted in Figure 1. Although the excitation volume is very small, resonance phenomena are responsible for intense and sharp Raman bands (Dresselhaus et al. 2007). In the case of SWCNTs, the specificity in Raman vibrational activity is summarised in the aforementioned splitting of the G line and the presence of the Radial Breathing Mode (RBM) which is both dispersive and characteristic of the carbon nanotube diameter. The RBM corresponds to the out-of-plane stretching or the radial breathing of the graphitic structure (Dresselhaus et al. 2005). The RBM

frequency is inversely proportional to the SWCNT diameter, a property which stems directly from the moment of inertia or the carbon mass distribution around the nanotube axis. Fundamental to the characterisation of SWCNT using Raman spectroscopy is the dependence of the RBM on the excitation frequency, which gives rise to the Kataura plot (Kataura et al. 1999), see Figure 2. This corresponds to different resonant properties of nanotubes of different diameters, which in their turn allow for the probing of the existence of "single molecule" structures within the bulk of multiple nanotube morphologies (Dresselhaus et al. 2005). In other words, the spectral information contained in a spectrum for a given excitation energy corresponds to the fraction of the nanotubes that are in resonance with the specific laser line (Milnera et al. 2000) which can even be assigned to a specific chirality (Jorio et al. 2001). The RBM feature is associated with small nanotube diameters, and thus is disappearing for Multi-Wall Nanotubes, although its presence has been reported under good resonance conditions (Benoit et al. 2002).

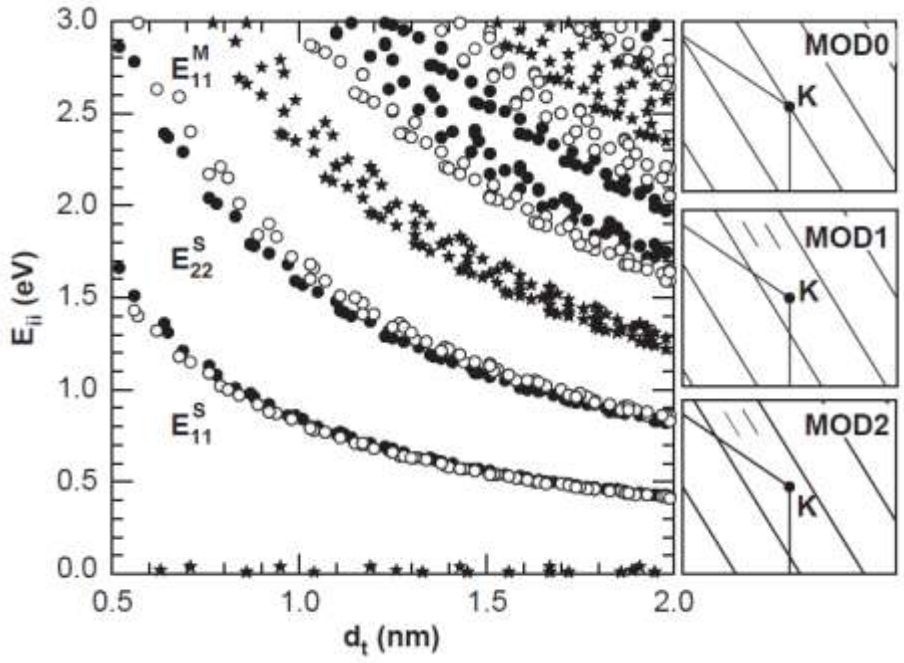

Figure 2: The Kataura plot shows the transition energies vs. SWCNT diameter. The right panels show schematic figures defining the SWCNT classes (Reprinted from (Dresselhaus et al.), with permission from Elsevier)

As aforementioned, SWCNTs present distinct features in the G line. This is attributed to the lifting of the degeneracy of the E_{2g} due to its tubular symmetry. Typical of the

Raman spectrum of SWNTs is the presence of the G^- and the G^+ lines which correspond to the axial and circumferential vibrations of the rolled graphene sheet. Whereas G+ is sensitive to the presence of dopants (Dresselhaus,Dresselhaus 1981), G^- is sensitive to the nature of the tube i.e. metallic or semiconducting but not on the chirality (Pimenta et al. 1998), (Brown et al. 2001). Both G lines are reported to be formed from three peaks from different symmetries which are polarisation dependent (Jorio et al. 2000), (Jorio et al. 2003), raising the number of vibrational modes that form the G line to 6 (2A, 2E1 and 2E2).

Finally, the second-order Raman spectrum is dominated by the feature at approximately 2700 cm^{-1}. The so-called G' line is a double resonance process and is related to the D band at 1350 cm^{-1}, or the disorder induced band. The D band is a single phonon process and the G' prime band is a dual phonon double resonance process. In the case of graphite, the D band can be fitted with two Lorentzian distributions, whereas the G' band can be fitted with one Lorentzian (Can et al. 2002), a fact that renders the specific line especially attractive for stress monitoring. As in the case of the D line, the G' band is related to diameter and chirality. This is attributed to the fact that as the planar structure is converted to a tubular one in the case of CNTs, the bandwidth of these spectral lines are directly affected (Jorio et al. 2002). However, as has been reported (Souza Filho et al. 2002), whereas in the majority of graphitic structures, the G' appears as a single distribution, in the case of individual SWCNTs, a two-peak vibrational activity has been reported. This vibrational activity is related to the electronic properties of the nanotube and is associated to distinct resonance processes sufficiently separated in resonance energy. Other cases where the G' line presents a morphology that diverges from a single distribution are attributed to interlayer coupling (Malard et al. 2009a), tunnelling effects (Cui et al. 2009) etc. Other vibrational modes are also reported which include overtones and combination modes like the 1750 cm^{-1} band, the iTOLA combination mode at the area of 1800 cm^{-1} to 2000 cm^{-1}, or the intermediate frequency modes IFMs with frequencies that range between the RBM and the G mode (Figure 1).

As previously stated, for multi-wall CNTs (MWCNTs), all the aforementioned features that distinguish SWCNTs from other graphitic structures tend to disappear and the spectrum converges to that of turbostratic graphite (Cançado et al. 2008). However, specific features have been reported which include the splitting of the G band which relates to the presence of very small diameter inner tubes (Benoit et al.

2002), the dual morphology of the G' band which relates to the circumferential deformation of the tube particularly for double-wall CNTs (Bandow et al. 2004), or the presence of the RBM under specific resonance conditions (Pfeiffer et al. 2003).

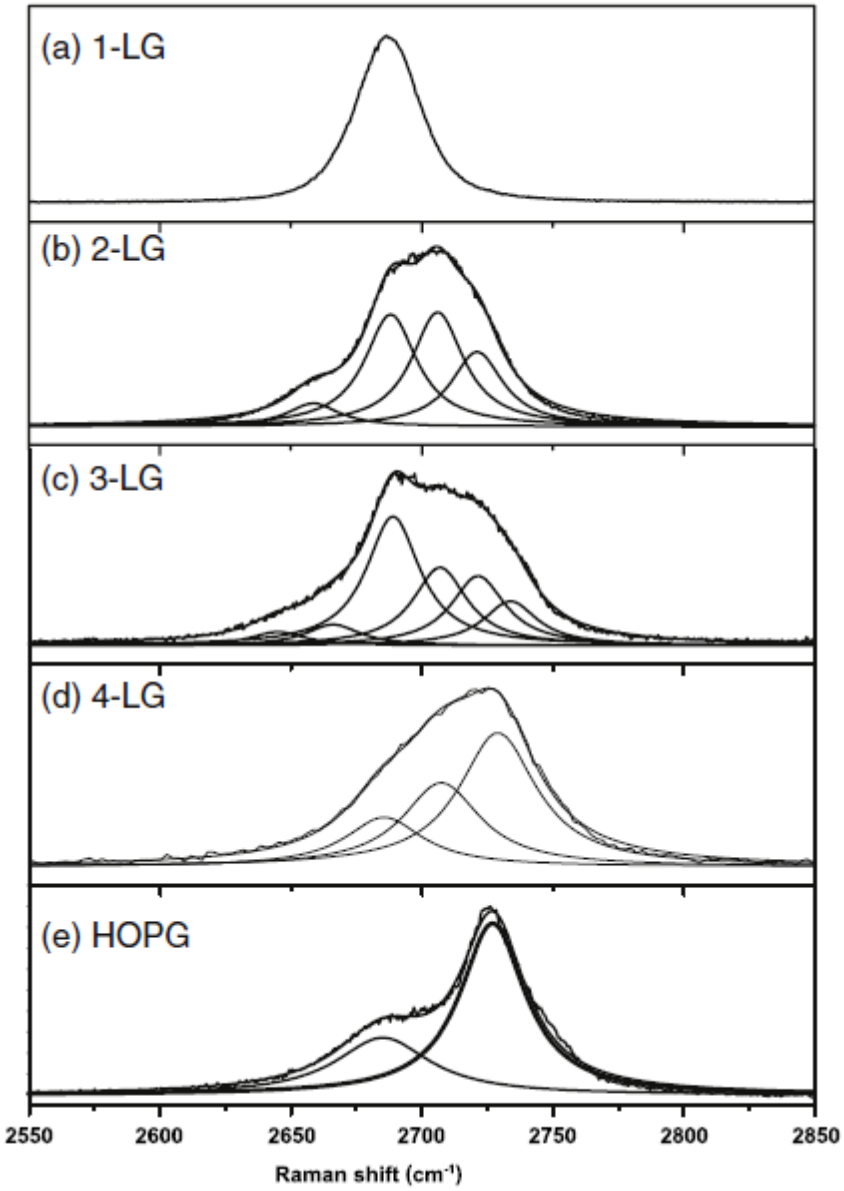

Figure 3: The measured G' Raman band with 2.41 eV laser energy for (a) 1-LG, (b) 2-LG, (c) 3-LG, (d) 4-LG, (e) HOPG (Reprinted from (Malard et al.), with permission from Elsevier).

Last but not least, graphene has recently been in the focal spot of the international research community. Being the simplest sp^2 Carbon structure or else the basic building unit of any graphitic structure, graphene is ideal for evaluation and further investigation using Raman Spectroscopy. Monolayer graphene is unique in that the G' line is remarkably more intense than the G line and this can be understood in terms of

a triple resonance process (Malard et al. 2009b). As more graphene layers are added to the structure, the G' line transforms from a simple Lorentzian to a more complex peak, where more than one lines appear to coexist due to the interlayer interaction (Figure 3). The complexity of the peak is attributed to the interlayer interaction and the random rotation along the c axis of the graphene layer (Malard et al. 2009a). Interestingly enough, turbostratic graphite where rotational effects are minimised, also exhibits a single Lorentzian morphology. However, this is upshifted in frequency and is wider and of lesser intensity than the corresponding G line (Cançado et al. 2008). Of particular interest is the emergence and morphology of the disorder lines, as different types of graphene edges are probed (Malard et al. 2009b).

6.3. Stress dependence of the Raman Spectrum

6.3.1. The principle

There are *3**N**-6* possible vibrations in the general case of a polyatomic molecule. Each one corresponds to an internal displacement co-ordinate. In the purely linear elastic case, the displacement may be regarded as directly proportional to the restoring force. The *3**N**-6* set of constants of proportionality are called the force constants. In this case, all vibrations are purely harmonic and the potential energy of the system is the sum of the quadratic terms whose coefficients are the force constants.

For one simple vibrational motion, according to the above,

$$\boldsymbol{F} = k\,(x-x_0) \qquad (1)$$

where $\boldsymbol{F}$ is the restoring force, k is the force constant, and $(x-x_0)$ is the distance from the equilibrium position x_0. Integrating equation 1 with respect to x provides the potential energy function U_p:

$$U_p = \frac{1}{2}k\,(x - x_0)^2 \qquad (2)$$

which is the parabola shown in Figure 4a. This oscillation is harmonic and its frequency ν is independent on the distance from the position of equilibrium x_0. The

quantum theory of the harmonic oscillator only allows one transition from one energy state to another $\Delta v = \pm 1$. These energy states are shown as dotted lines in Figure 4a and are equidistant.

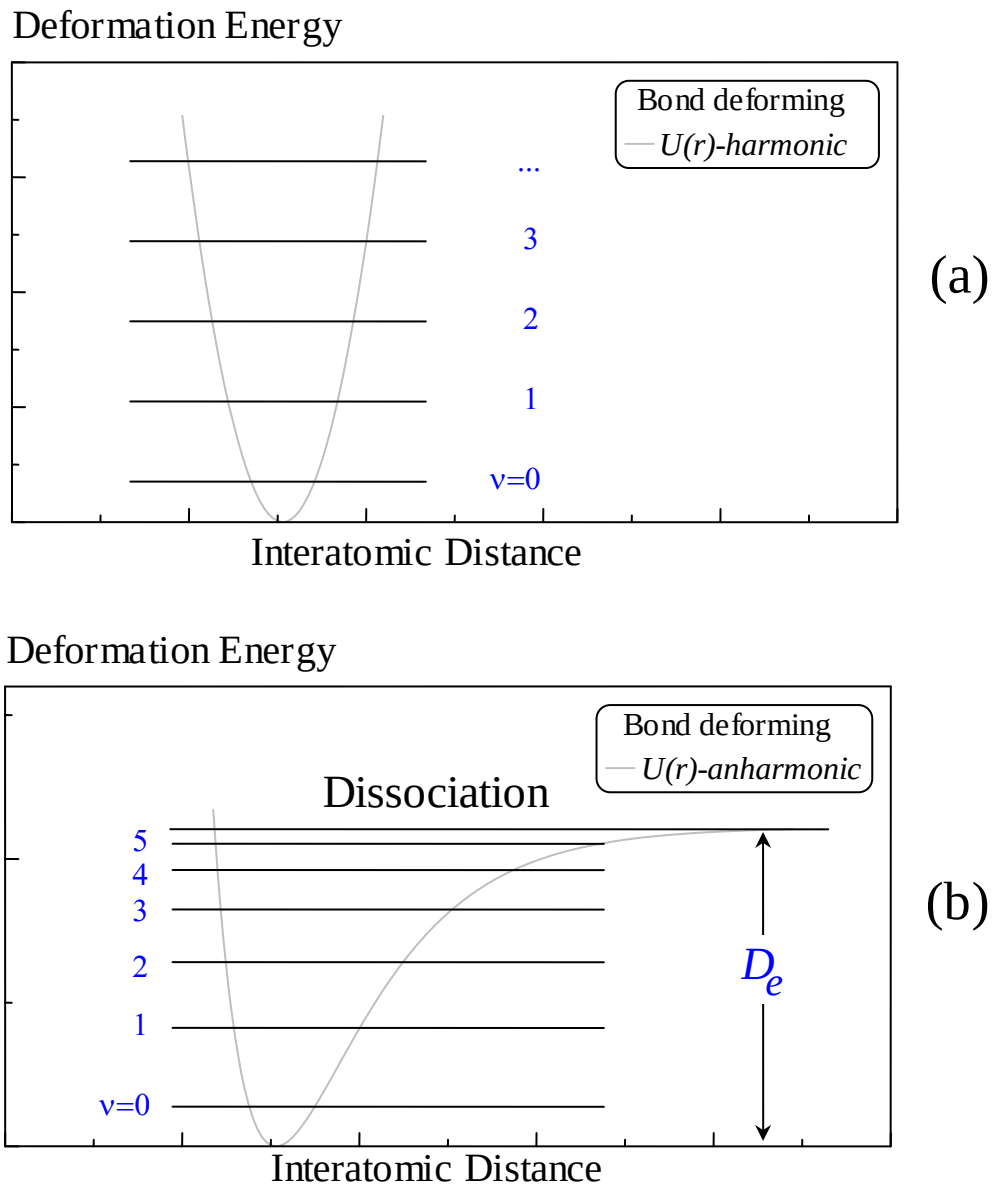

Figure 4: (a) The potential energy function U_p for the Harmonic Oscillator. The dotted lines mark the allowable energy levels and are equidistant. (b) The potential energy function U_p for the Anharmonic Oscillator. The dotted lines mark the allowable energy levels and are no longer equidistant.

It is, however, well known that phenomena like overtones, combination bands, or difference bands (Colthup 1975) cannot be explained by the simplistic harmonic

theory. In addition, concepts like bond breaking at high deformations demand a different approach to the potential energy function. Such an approximation is the *Morse function*, where the potential energy is a function of the dissociation energy D_e, or the energy required to break the bond:

$$U_p = D_e(1 - e^{-b(x-x_0)})^2 \qquad (3)$$

where b is a constant.

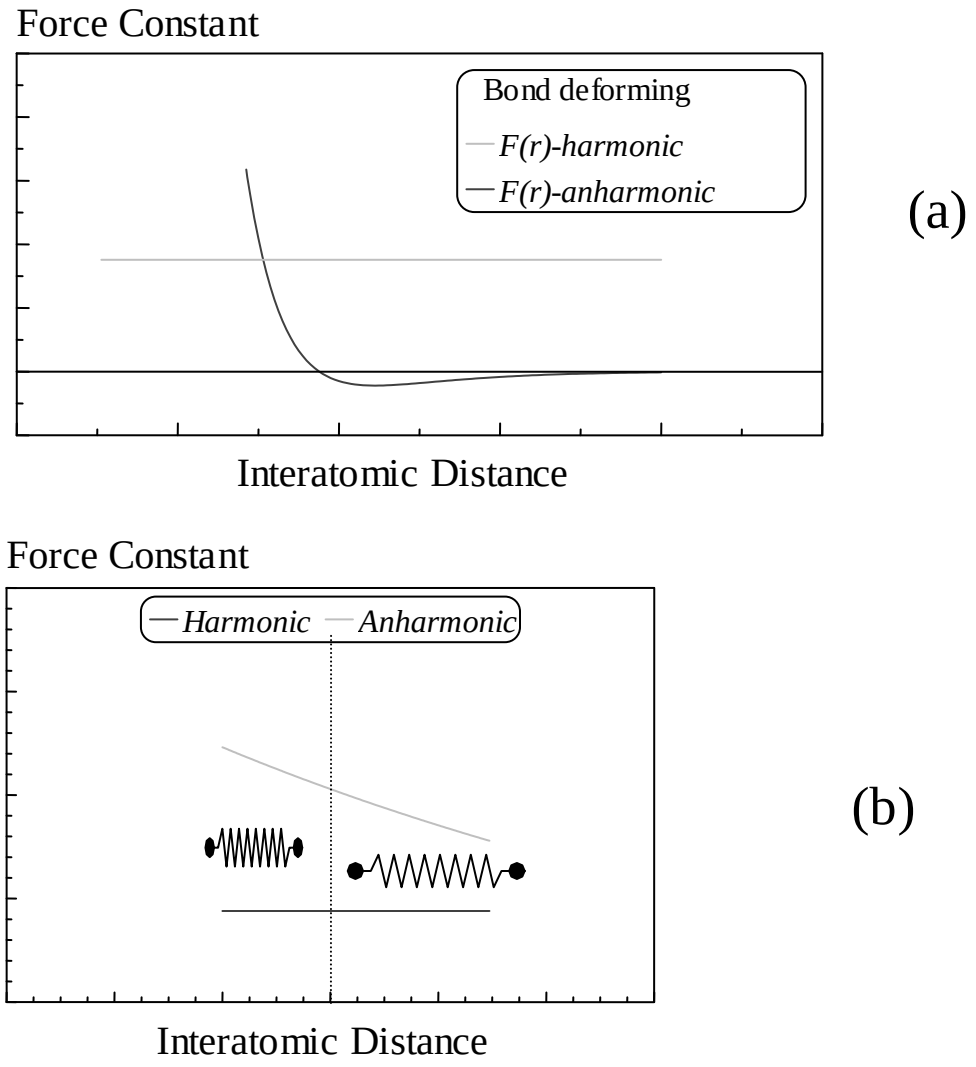

Figure 5: (a) the variation of the force constant as a function of interatomic distance; (b) for small displacements, the stress dependence may be regarded to a good approximation as proportional to the molecular deformation.

In Figure 4b, the potential energy of the anharmonic oscillator is depicted. The dotted lines represent the allowable energy levels. The quantum theory accounts for more than one transition between energy levels.

6.3.2 Stress dependence of the vibrational frequency

The second derivative of the Morse anharmonic potential energy function provides the equation for the force constant (Tashiro et al. 1990):

$$k = 2b^2 D_e (2e^{-2b(x-x_0)} - e^{-b(x-x_0)}) \quad (4)$$

As can be seen, the force constant is no longer a constant in the anharmonic case. Moreover, it is a function of the internuclear displacement and its dependence is depicted in Figure 5a. For small positive internuclear displacements, $x = x\text{-}x_0 > 0$, the force constant is monotonically decreasing. For positions near the equilibrium, the Morse function resembles the harmonic oscillator function, and the frequency ν can be regarded as proportional to $\sqrt{k}$ (Colthup 1975), (Tashiro et al. 1990). This results in a low frequency shift $\Delta\nu$ of the vibration. On the other hand, when the bond is compressed, that is when $\Delta x < 0$, the force constant increases causing a high frequency shift $\Delta\nu$.

The above principle provides the theoretical background for the frequency shift of distinct Raman bands when the molecule is subjected to external load. The theoretical calculation of the expected shift $\Delta\nu$ has been presented for simple molecules (Wool 1980), (Tashiro et al. 1990). More complicated analyses include the lattice dynamical theory to predict stress induced shifts in polymer chains.

For small displacements (Figure 5b), the stress dependence may be regarded to a good approximation as proportional to the applied stress field σ. Bretzlaff and Wool (Bretzlaff,Wool 1983) propose the following:

$$\Delta\nu = a_\sigma \sigma \quad (5)$$

where a_σ is the proportionality constant.

The key feature that links the stress dependence of the molecule to any macroscopic deformation is whether this deformation affects the material at a molecular level. Whereas amorphous materials are not expected to show detectable

stress sensitivity, highly crystalline materials, such as Kevlar® (Galiotis et al. 1985) or carbon (Robinson et al. 1987), are reported to exhibit measurable stress sensitivity. Provided that a suitable reference value is given for the unstressed material, experimental calibration curves may be employed to translate Raman frequency shifts to absolute strain. In most cases, a direct proportionality of the shift to the applied strain is adequate (Galiotis et al. 1983), although higher order dependence has been proposed in the literature to account for non-linear elastic behaviour (Melanitis et al. 1994).

What is of particular interest is that the shift of a strained bond is expected to be proportional to the bond deformation, or else that there is a direct relationship between the stress induced Raman shift and the bond stiffness or the Young's modulus of a macroscopic structure (Gouadec,Colomban 2007). These relationships allow for universal plots that correlate the strain induced Raman Shift with the moduli of known fibres, see Figure 6.

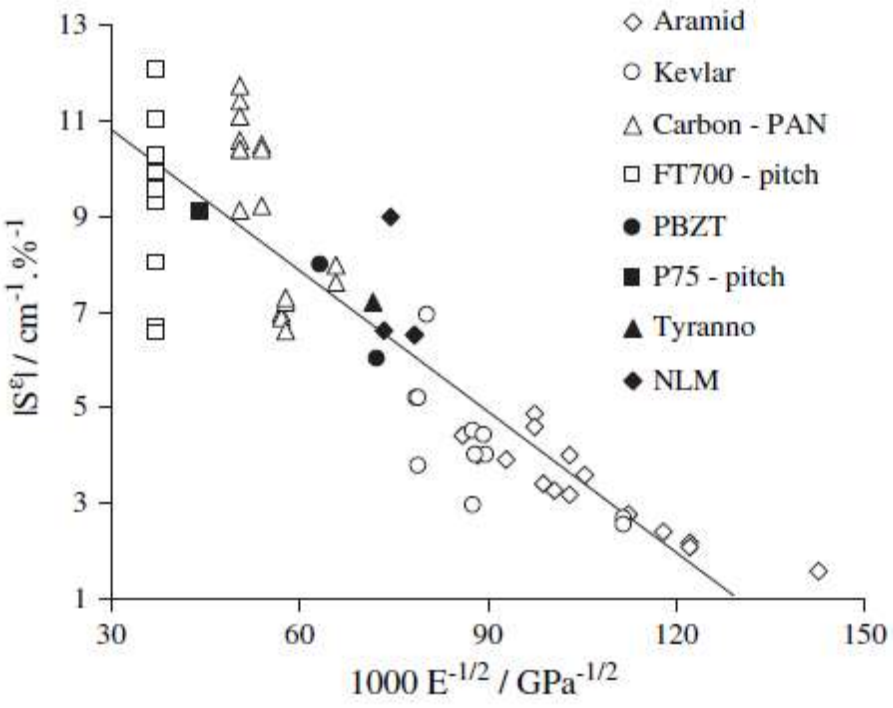

Figure 6: Stress dependent shift of the G band vs. the inverse of Young's modulus square root (Reprinted from (Gouadec,Colomban), with permission from Elsevier).

6.4. Stress induced changes in the Raman spectrum of Graphitic structures

The application of stress in graphitic structures is limited by the size of the structure in that there must be an adequate means of transferring the stress. For this reason, although a lot of effort has been invested in the stress dependence of the Raman spectrum in structures of micron dimensional order such as carbon fibres, there is limited reported research on direct application of stress on CNTs. However, a lot of research effort has been associated with the behaviour of graphitic structures under pressure (hydrostatic or not). This section will focus on the direct stress application on graphitic structures.

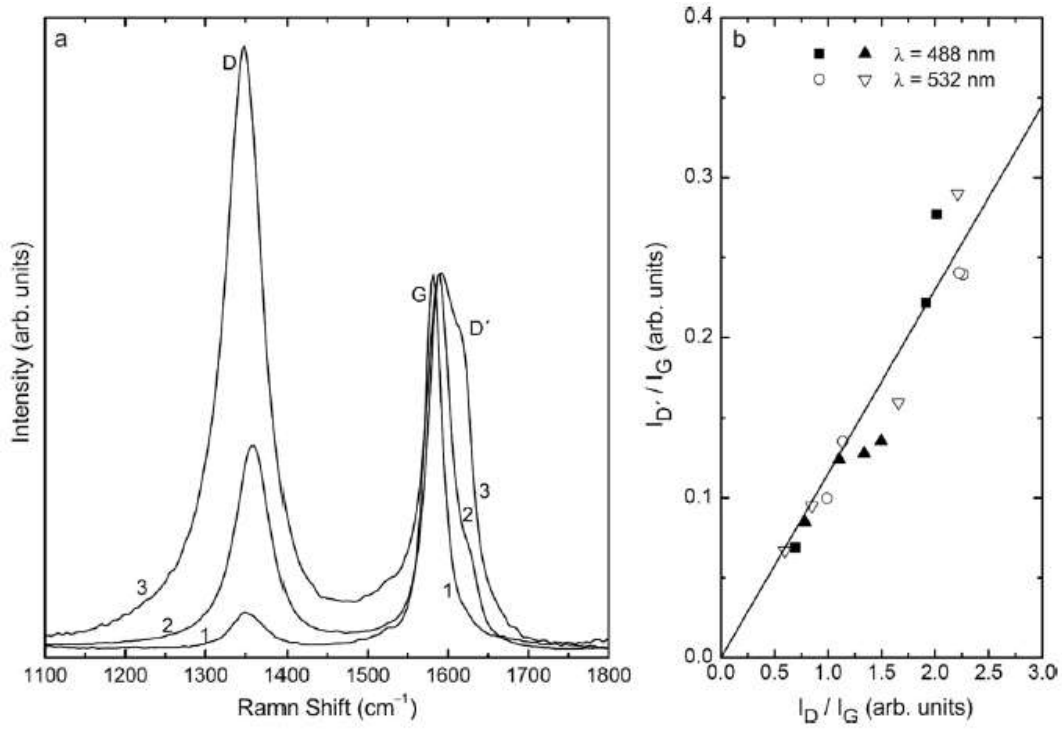

Figure 7: (a) Raman spectra of a HOPG sample at three selected stresses (1, 2 and 0 GPa, respectively). (b) Ratio of the D'/G band intensities as a function of the ratio of the D/G band intensities (Reprinted from (del Corro et al.), with permission from Elsevier).

Early works focus on the application of pressure on single crystal graphitic structures and reveal considerable frequency upshift of both E_{2g} Raman active modes (at ~50 and 1580 cm^{-1}). Hanfland et al report this upshift and correlate it to the structural

deformation of the Graphitic crystal due to the strong anharmonicity of the C-C bond (Hanfland et al. 1989). In a recent work, Del Corro et al. employed a moissanite anvil cell coupled to a Raman microscope to monitor the evolution of distinct Raman bands of highly oriented pyrolytic graphite (HOPG) under non-hydrostatic pressure conditions. The employment of the moissanite cell instead of the typical diamond one allowed for monitoring of the shift of the D band (Del Corro et al. 2008). Figure 7 depicts the Raman spectra of a HOPG sample at three selected stresses and the Ratio of the D'/G band intensities as a function of the ratio of the D/G band intensities (del Corro et al. 2011).

The stress induced changes in the Raman spectrum of Carbon fibres have been thoroughly studied, as Carbon Fibres are almost ideal for direct axial stress application. The first and second order Raman vibrational modes of high modulus fibres exhibit considerable shift with strain. As has been reported, the vibrational modes D, G and G' exhibit strain dependence of approximately 7, 9 and 17 cm^{-1}/% respectively (Galiotis,Batchelder 1988). The considerable shift of the G' band was as expected for a second-order feature and was correlated with the shift of the D band. The study of the spectroscopic behaviour of Carbon Fibres has been extended to compression via application of the Cantilever Beam Technique (Melanitis,Galiotis 1990). The deviation from non-linearity when the fibres are stressed in compression was attributed to the microscopic buckling of the graphene layers which was even reversible in the case of low modulus carbon fibres (Melanitis et al. 1994). For this reason, the technique may be employed for the determination of the compressive strength of individual fibres. As should be noted, the lower the graphitization of the Carbon Fibre, the harder it is to monitor the strain induced changes, as on one hand the disorder features increase in full width at Half Maximum (FWHM) and intensity relative to the G line and on the other hand the second order G' line is not readily detectable (Melanitis et al. 1996). As postulated in the previous section, a direct relation between the modulus and the phonon frequency is expected, and therefore every Raman active bond should have a unique stress dependence. In this respect, Raman Frequency vs. stress calibration curves are more characteristic than Raman Frequency vs. strain calibrations (Paipetis,Galiotis 1996).

As aforementioned, the Raman study of sp^2 graphitic structures of nano scale such as CNTs, imposes restrictions in terms of the load application. Various researchers have focused on the induced Raman shifts with applied pressure. Sandler et al (2003) report

on the pressure dependence of the Raman modes of various carbon nanostructures such as different types of CNTs, graphite crystals and nano-fibres and compare their findings to the behaviour of high modulus carbon fibres. As expected, the Raman modes were found to shift reversibly to higher wave numbers with pressure. The authors used the polarization dependence of the strain induced Raman shift to predict the initial pressure dependence of all tested nanostructures and identified a reversible collapse condition for hollow nanostructures.

The Raman spectra of novel graphitic spheres identified as a side product of fullerene synthesis have been found to be similar to that of micro-crystalline graphite (Loa et al. 2001). The authors report that the silent low-frequency $B_{1g}(1)$ phonon of graphite becomes Raman active and that high pressure affects the G' mode near 2700 cm^{-1} which exhibits a peculiar dispersive behaviour.

The pressure evolution of the Raman spectrum of stacked-up carbon nanofibres which exhibit a unique morphology of stacked conical graphene cups along the fibre axis revealed a -3 cm^{-1}/GPa dependence for the D' double resonance feature and -4.2 cm^{-1} /GPa for the graphitic G line (Papagelis et al. 2011). The authors report the merging of the G and D' line which is indicative of the differential pressure dependence of the two Raman bands.

Carbon onions and nanocapsules exhibit similar behaviour to that of MWCNTs (Guo et al. 2009). The special characteristic of these structures is that they can sustain very high pressures prior to collapsing. However, differences in the pressure induced shifts between compression and decompression were attributed to structural damage of the nanostructures.

As aforementioned, the Raman Spectrum of more elaborate sp^2 structures possesses intrinsic characteristics. Apart from the inverse dependence of Raman bands to stress application, the Raman response of such structures may be more complicated. Relatively early studies report pressure induced changes in the Raman spectrum with an anomalous behavior in the pressure range of 10 -16 GPa (Teredesai et al. 2000). The authors suggest that the intensity changes are attributed to pressure induced deviation from resonance conditions. The reported softening is attributed (i) to diameter dependent collapse of a fraction of the studied tubes and (ii) to the influence of the pressure medium which may penetrate the tube. The effect of the pressure medium is also identified in other studies (Dunstan,Ghandour 2009), where the nature

of the pressure medium as well as the resonance effects with Raman excitation energy are reported to be of major importance.

The Raman spectroscopy of filled double-wall CNTs (DWCNTs) with trigonal Tellurium revealed red shift of the G' band attributed to the softening of the C-C bonds upon capillary filling of the tubes. (Belandria et al. 2010). The authors employed the capillary filling of the tube to distinguish pressure induced changes between the inner and the outer wall and verified that in the presence of Te, the pressure coefficients of the G band of the internal and the external CNTs are larger than in the case of empty DWCNTs.

The Raman spectrum of metallic SWCNTs and DWCNTs under high pressure exhibits a variety of pressure induced changes. These include the deformation of SWCNTs and the DWCNT outer tubes, the quasi-isolation of the inner tubes as well as a narrowing of the characteristic Breit–Wigner–Fano Raman peak attributed to tube –tube interactions at high pressures (Christofilos et al. 2006). In Figure 8, the distinct changes in the frequency area 1350 to 1700 cm^{-1} are depicted.

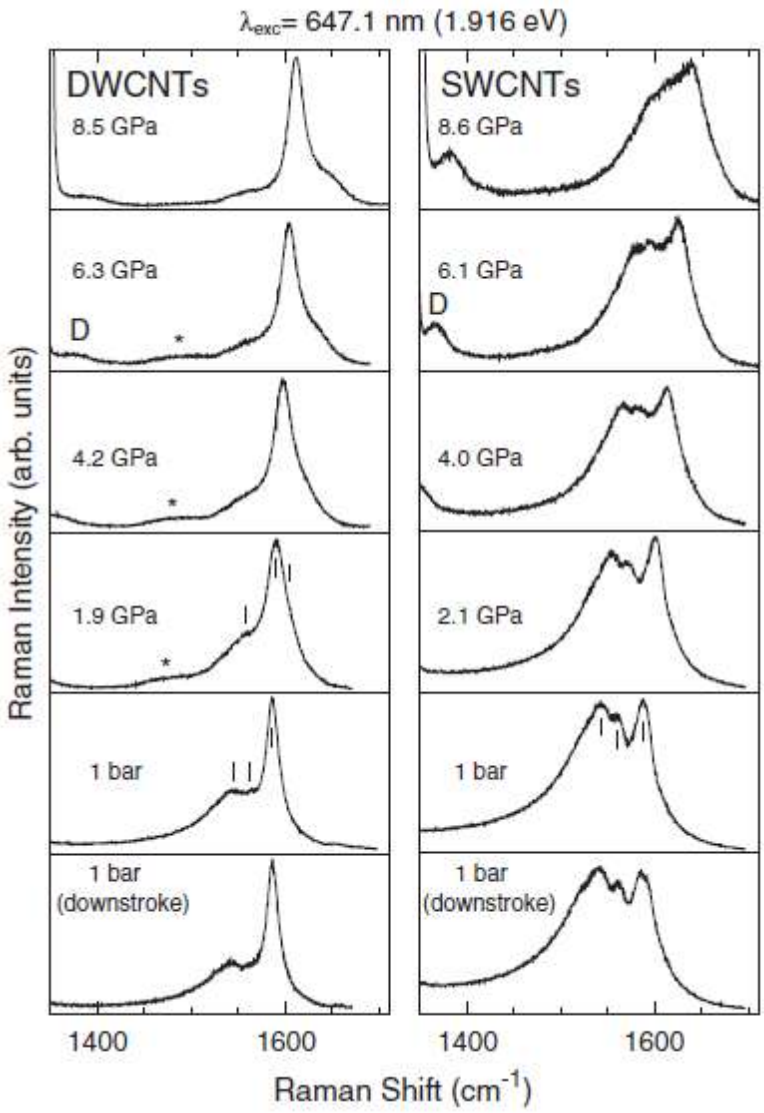

Figure 8: Raman spectra of DWCNTs (left panel) and SWCNTs (right panel) in the G band frequency region at room temperature and for various pressures. Vertical lines denote the main G-band components, ''D'' refers to the nanotube D-band, while asterisks mark a methanol–ethanol band (Reprinted from (Christofilos et al.), with permission from Elsevier).

Venkateswaran et al have studied the pressure dependence of RBM and G vibrational modes of purified and solubilised SWCNTs and reported that an abrupt drop in the intensity of these bands is seen near 2 GPa, which suggested a phase transition. The authors identified a 10 cm^{-1} upshift in the RBM of the purified SWCNTs compared to the as-received SWCNTs. Pressure induced changes were reversible and the pressure dependence of the RBM and G bands was significantly influenced by the changes in the electronic structure (Venkateswaran et al. 2001).

The second-order Raman G′ band of bundled DWCNTs and SWCNTs exhibited different pressure behaviour. The applied pressure induces a splitting of the G' peak in the case of DWCNTs (Papagelis et al. 2007). In the latter case, the distinct components of the G' vibrational mode are identified and associated with the inner and the outer tube diameter of the resonantly probed tubes and the strength of the inner-outer tube interaction. Moreover, the authors identify a dependence of the pressure induced Raman Shift to the laser wavelength which they attribute to the sampling volume of the excitation wavelength. The effect of the inner –outer tube interaction has also been verified for increased laser powers (Puech et al. 2011).

The effect of high-pressure on the Raman Spectrum has also been studied in the case of monolayer, bilayer, and few-layer graphene samples supported on silicon (Proctor et al. 2009). The authors report that the pressure dependence tends to that of unsupported graphite with increasing graphene layers and attribute this finding to the fact that the compressive behaviour is dominated by the stiffness of the substrate.

Although there is comparatively extended research effort in the area of high pressure of sp^2 carbonaceous structures, a limited number of studies exist on the direct stress application on nano-scaled graphitic structures. Cronin et al managed to strain individual SWCNTs by using an atomic force microscope tip and at the same time interrogating the strained tube with a Raman microprobe (Cronin et al. 2004). The SWCNT was deposited on SiO2 and secured in place using electron beam lithography. The authors secured the uniformity in chirality and diameter by scanning along the length of the individual interrogated nanotube. The authors report remarkable redshifts of the D, G and G' bands with applied strain, i.e. 27, 14 and 40 cm^{-1} whereas no shift in the RBM is reported. The intensity of the RBM varies with strain due to relaxing of the resonance conditions. In a later work (Cronin et al. 2005), the authors report on the chirality dependence of the stress induced shift and report that semiconducting SWCNTs remain resonant with the window of applied strain whereas metallic SWCNTs move in and out of resonance with strain, indicating a strain induced shifting of the electronic subbands.

Elaborate studies of the chirality dependence on strain induced shift are performed in the work presented by Gao et al (Gao et al. 2008). In this work, individual SWCNTs are transferred on a polymethylsiloxane flexible scaffold and fixed in position by gold deposition (Figure 9). Subsequent straining of the scaffold strains the individual SWCNTs. The authors report on the G line mode splitting due to applied strain (figure

10). Increasing Chiral angle is found to affect significantly the blue shift rate of the Raman G^- and G^+ line. The authors also report on the redshift of the IFM which is not consistent with the bond softening principle described in the previous section. Liu et al (Liu et al. 2009) provide an extensive overview of the effect of various stress fields on SWCNTs.

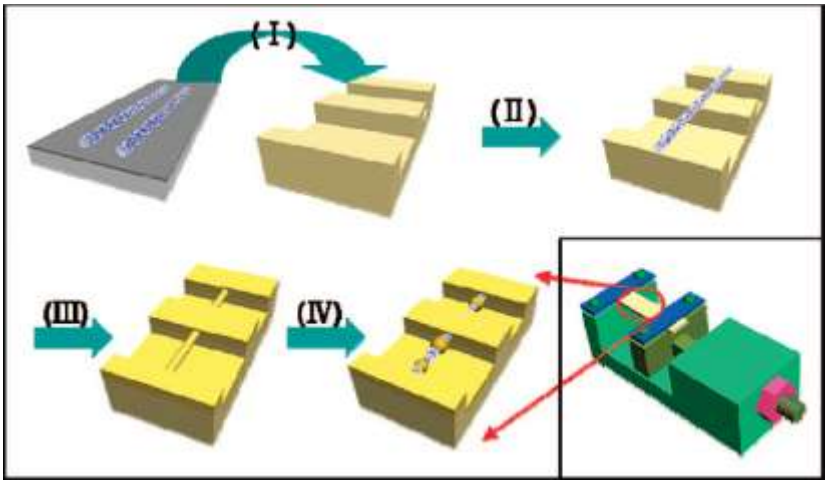

Figure 9: Schematic drawing of the method for SWCNT tensile testing (Reprinted with permission from (Gao et al.). Copyright 2008 American Chemical Society).

As mentioned above, graphene is the simplest of all sp^2 graphitic structures and at the same time their building unit. Recent experimental work on graphene under stress reveals the splitting of the G' band (Figure11) which depends on the polarization of the excitation light, as well as the direction of stress (Frank et al. 2011a).The authors attribute the mode splitting to (i) the induced asymmetry of the Brillouin zone (ii) the additional contribution of the inner double resonance mechanism and (iii) the laser polarization with respect to the loading axis. The method to experimentally apply strain on the graphene layers was the cantilever beam method, where a clamped elastic beam is subjected to strain causing a strain gradient along its length. The graphene layer is attached to the surface of the beam. The support provided by this attachment allows for applying six times higher compressive strains than in the case of suspended graphene, prior to buckling (Frank et al. 2010). The study of graphene allows for the determination of a single stress factor or stress dependence of the Raman Frequency. This corresponds to the C-C bond stiffness and should be the limit of all sp^2 graphitic structures as stress is transferred from the far field to the C-C bond

(Frank et al. 2011b). The universal value that is characteristic of the graphitic band was calculated to be approximately 5 cm^{-1}/ MPa.

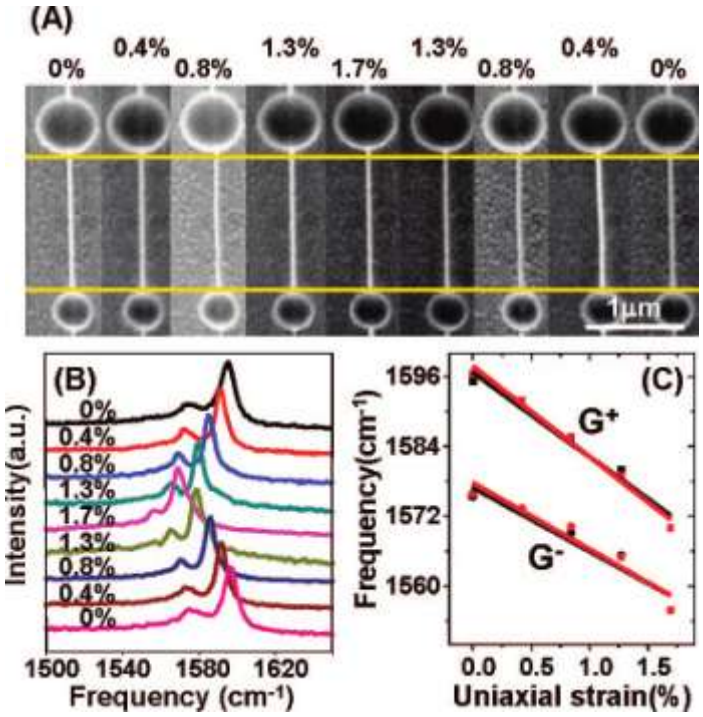

Figure 10: (A) SEM image, (B) G-band spectra of (18, 5) SWNT when uniaxial strain first increases from 0% to 1.7% and then decreases to 0%. (C) G^+ and G^- frequencies variation as a function of uniaxial strain (reproduced from (Gao et al.)) (Reprinted with permission from (Gao et al.). Copyright 2008 American Chemical Society).

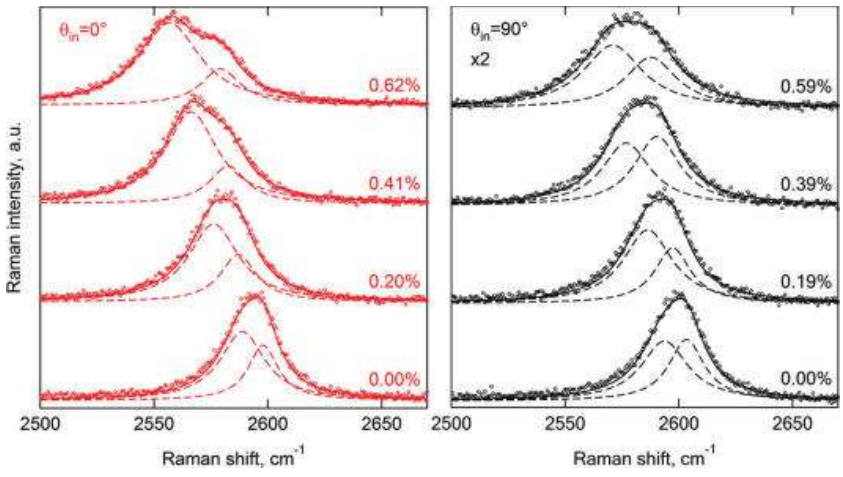

Figure 11: Raman G' band splitting under strain in graphene for parallel and vertical polarization with respect to the loading axis (Reprinted with permission from (Frank et al.). Copyright 2008 American Chemical Society).

6.5. Stress transfer Raman Studies in composites reinforced with sp^2 graphitic nanostructures.

It is beyond any doubt that the stress transfer between the matrix and the reinforcing phase is of primary importance in the structural behaviour of reinforced composites. Raman microscopy has been employed for over two decades for monitoring the interface at microscopic level between graphitic materials and polymer matrices. The dependence of the Raman modes on applied stress allows for the local stress monitoring at a resolution which is practically only limited by the diffraction limit of the excitation wavelength λ, i.e. $\lambda/2$. The current section is focusing on composite materials reinforced with sp^2 morphologies, with regards to micromechanics of reinforcement. These materials may be categorized in terms of their dimensionality, or in other words the anisotropy of the nano-reinforcement which in its turn is controlled by the alignment of the nanophase in space. In this respect, macroscopic nano-graphitic structures may be 1D, like typical nano-fibres (Vigolo et al. 2000) which are by definition transversely isotropic, 2D, like bucky papers (Bahr et al. 2001) which may be employed to form orthotropic laminates, or 3D composite systems which are isotropic in the macro-scale (Coleman et al. 2006).

As aforementioned, the difficulty of handling and aligning the nano-dimensional phase is not an issue in the case of carbon fibres (diameter in the order of 10 micron and practically unlimited length). Carbon fibres are the first sp^2 carbon structures studied as reinforcing phase in structural components using Raman Microscopy. Aligned carbon fibres in model single fibre composites (Paipetis,Galiotis 2001), model multi-fibre composites (Galiotis et al. 1996) or even typical laminates (Chohan,Galiotis 1997) have been probed in order to study the efficiency of the stress transfer (Paipetis,Galiotis 1997), the effect of neighbouring fibres (Van Den Heuvel et al. 1997), and the stress redistribution after a fibre break (Marston et al. 1996). The acquired stress profiles have been associated with the integrity, the stiffness and the toughness of the interface (Yallee,Young 1998) and analytical models have been employed to model the axial and shear stress profiles at the interface (Paipetis et al. 1999).

The load transfer in CNT reinforced matrices is by far more complicated as it encompasses a variety of parameters which include dispersion, agglomeration,

wetability, aspect ratio, alignment, and morphology. In other words there are a lot of prerequisites that have to be satisfied before the nanocomposite can be regarded as a macroscopically isotropic short fibre reinforced composite. The first published work on the Raman investigation of the load transfer in CNT reinforced composites (Schadler et al. 1998) reports a considerable shift in compression of the G' band of multi-all nanotubes (approximately 7 cm^{-1}/%). This was not the same for the same nanocomposites in tension, where although the shift was slightly positive, the experimental scatter could not allow for direct conclusions. The authors attribute this observation to either poor bonding of the matrix and the nanotube surface or to weak bonding of the inner layers to the outer layer which leads to the sliding of the inner tubes with respect to the outer tube. The behaviour of the nano-composite in compression favours the second hypothesis, as geometrical constraints lead to the compressive deformation of all the tubular structure. Of course, the working hypothesis for this approach is that the stress induced Raman shift is averaged over the volume of the interrogated tubes. The reported stiffening of the epoxy matrix due to the MWCNT reinforcement is more prominent in compression than in tension but the difference is not as dramatic as in the case of the stress induced Raman Shift in tension and compression.

The first reported micromechanical test on individual CNTs is reported by Cooper et al, where CNTs bridging across holes in an epoxy matrix were pulled out from the epoxy matrix (Cooper et al. 2002). The authors employed the tip of a scanning probe microscope. A simultaneous recording of the applied forces allowed for a full force-displacement curve of the pull out process. The authors present a correlation between interfacial shear strength and the embedded length, to report that the interfacial shear strength falls with increasing embedded length, as is reported in single-fiber pullout tests. This is attributed to the fact that most of the shear stress transfer is occurring via the ‘‘ineffective length’’ (Pitkethly,Doble 1990). The authors claim that their findings support the hypothesis that the CNT polymer interface may be significantly stronger than the interface between fibre and matrix in typical systems such as glass or carbon fibre-reinforced composites. They attribute the enhanced adhesion to the existence of covalent bonds which arise from naturally occurring defect sites at the CNT wall.

Cooper et al studied the deformation micromechanics of both SWCNTs and MWCNTs embedded in epoxy matrix using Raman Spectroscopy and confirmed the blueshift of the Raman G' band with tension for all studied CNTs (Cooper et al.

2001). Interestingly enough, two different types of SWCNTs exhibit shifts that differ by an order of magnitude with macroscopically applied strain (Figure 12). This difference is attributed either to lower stiffness or to poorer dispersion of the tubes that exhibit the low shift. The second postulation is indicative of the effect that the dispersion, or the initial CNT morphology may have in the final nano-composite properties.

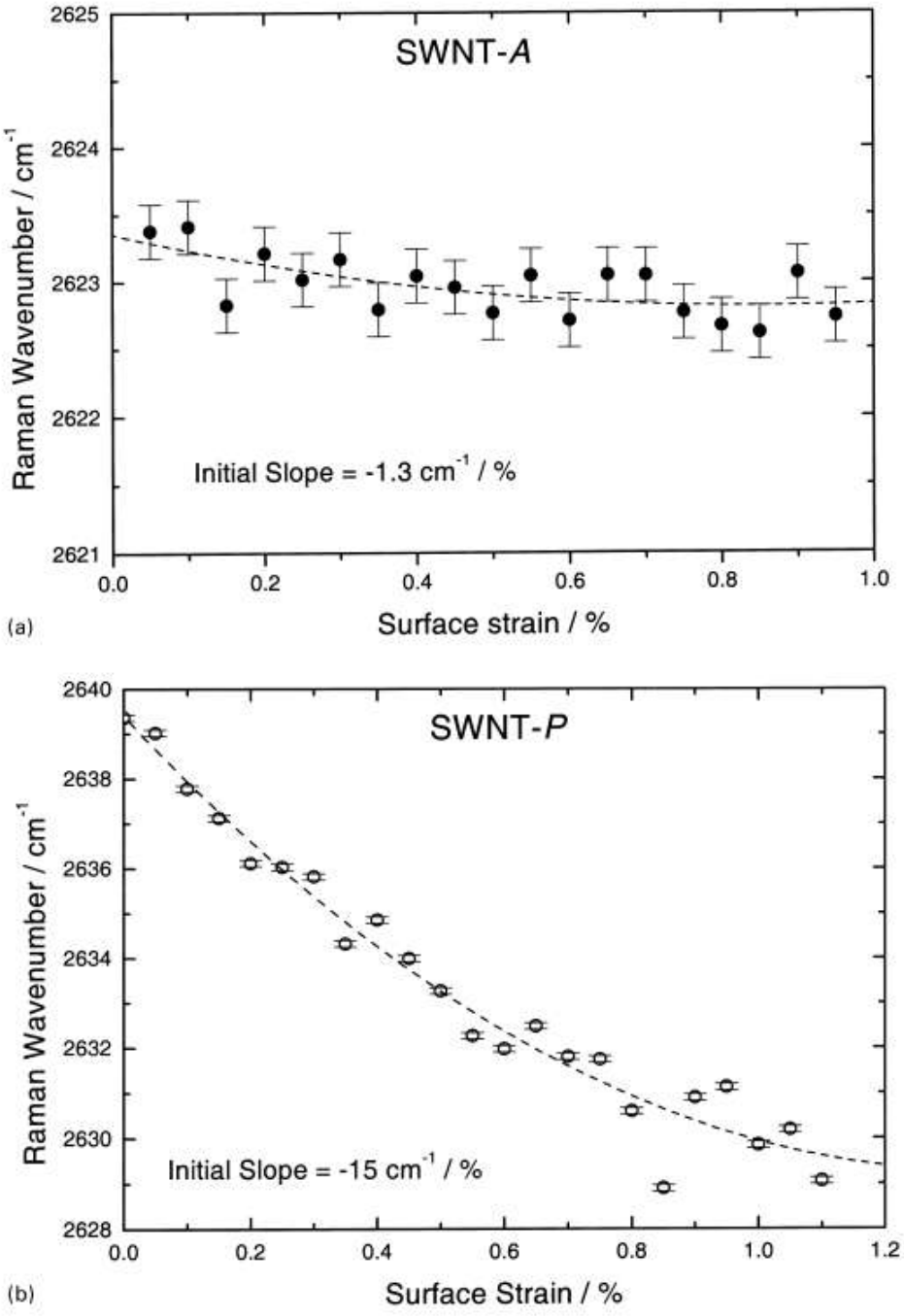

Figure 12: The strain induced shift differs by one order of magnitude for two different types of SWCNTs (Reprinted from (Cooper et al. 2002), with permission from Elsevier)

The authors assume that the nanotube-reinforced composites are short fibre reinforced composites with random reinforcement distribution and use well-known analytical formulations (Cox 1952), (Evans,Gibson 1986) to derive equivalent nanotube moduli for 2D and 3D distributions. The maximum calculated modulus of the reinforcing phase is found to vary between approximately 80 and 800 for 2D distribution of the reinforcement and between approximately 250 and 2500 for 3D distribution of the reinforcement. The 2D calculated values are regarded as more reasonable and the authors conclude that the moduli of 300 GPa and 1 TPa for MWCNTs and SWCNTs are in line with experimental measurement. However the huge discrepancy between the two kinds of SWCNTs is not adequately addressed. According to later stress studies on the chirality dependence of the stress sensitivity of SWCNTs (Gao et al. 2008), this discrepancy could also be attributed to other reasons than agglomeration and dispersion. As aforementioned, these studies reveal major differences in stress dependence for different types of CNTs (the strain induced shifts range from -4 cm^{-1}/% to -25 cm^{-1}/%, but they are calculated for the G^+ and G^- band and not for the G' as in the study by Cooper et al).

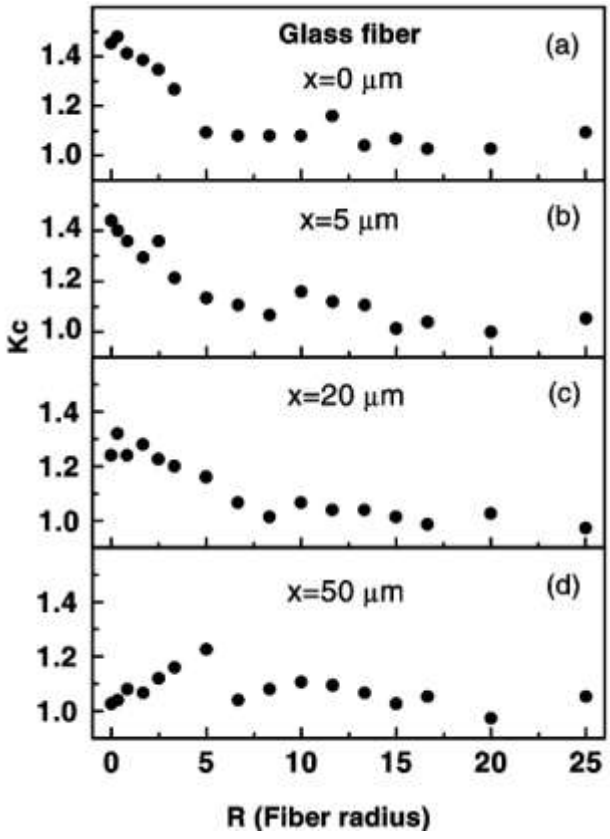

Figure 13: Strain in the carbon fibre (solid symbol) and in the CNT modified matrix near the fibre edge (open symbol) measured simultaneously by microRaman spectroscopy at applied stress levels of (a) 3 MPa, (b) 7 MPa, and (c) 10 MPa (Reprinted from (Zhao,Wagner 2003), with permission from Elsevier)

Zhao et al employed SWCNTs to monitor the stress concentrations around notches in nano-composites using polarized Raman Microscopy (Zhao et al. 2002) Using polarization studies with the polarization either vertical or perpendicular to the direction of the stress application they report that the polarization can be employed to interrogate nanotubes aligned in the polarization direction. In this case, the shifts of the G' band can be associated with the axial and transverse strain and calibration curves may be drawn. They observe a notable downshift with the polarization aligned to the stress application axis and an upshift in the transverse direction which they attribute to Poisson's contraction. The relative frequency shift when probing in the transverse direction away from the circular notch is associated with the stress concentration factor due to the notch. Similar stress concentration values were reported in a typical unidirectional aramid fibre composite laminate (Arjyal et al. 2000).

Furthermore, Zhao et al employed the same technique to monitor the stress field around the break of a two-dimensional model composite (Zhao,Wagner 2003). In their study, they modify a polymer matrix using SWCNTs and make single fibre model composites both with E-glass fibre and high modulus carbon fibre. They are successful in creating a stress contour map around the stress discontinuity invoked by the fibre break. In the case of a high modulus carbon fibre, they perform simultaneous mapping of the fibre and the modified matrix to produce "mirror" strain profiles associated with the fibre failure (zero stress at the vicinity of the crack) and the surrounding matrix (stress concentration at the vicinity of the crack (Figure 13). The same strain sensing principle is also employed in the case of E-glass polypropylene interfaces (Barber et al. 2004) and the measured data are associated with interfacial shear strength values calculated from the classical fragmentation test employing the Kelly-Tyson "constant shear" model (Kelly,Tyson 1965).

Kao and Young studied the combined effect of laser heating and deformation in the Raman shift of the G' band for SWCNTs in an epoxy matrix (Kao,Young 2004). As is reported in the case of carbon fibres (Everall et al. 1991), there is a downshift in the

G’ line with increasing laser power. They employ a four-point bending device to apply uniform strain at distinct increments and monitor the induced shift seamlessly in tension and compression. Unlike in the case of MWCNTs (Schadler et al. 1998), there is continuity in the slope of the transition region between tension and compression. Additionally, they report a plateau in the induced shift both in tension and in compression around 0.5% which they attribute to buckling and interfacial failure for compression and tension respectively. They also report on the influence of thermal stresses induced by the differential contraction between the matrix and the SWCNTs. By comparing a cold and hot curing matrix system they indicate that the presence of residual stresses favours stress transfer.

In a more recent work, Kao and Young (Kao,Young 2010) report a decrease in the stress transfer efficiency of CNT reinforced composites with cyclic loading. In particular they find that the stress sensitive G’ band is shifting with applied stress to lower wave numbers. The induced shift presents a hysteresis loop with cyclic loading and the authors correlate the hysteretic area to the dissipated energy (or to the induced damage at the interface), and normalize it to the total interfacial area between the nanotubes and the surrounding matrix. They employ reported experimental values from pull-out tests of individual nanotubes from a polymer matrix (Cooper et al. 2002) to evaluate interfacial damage of bundles and individual CNTs.

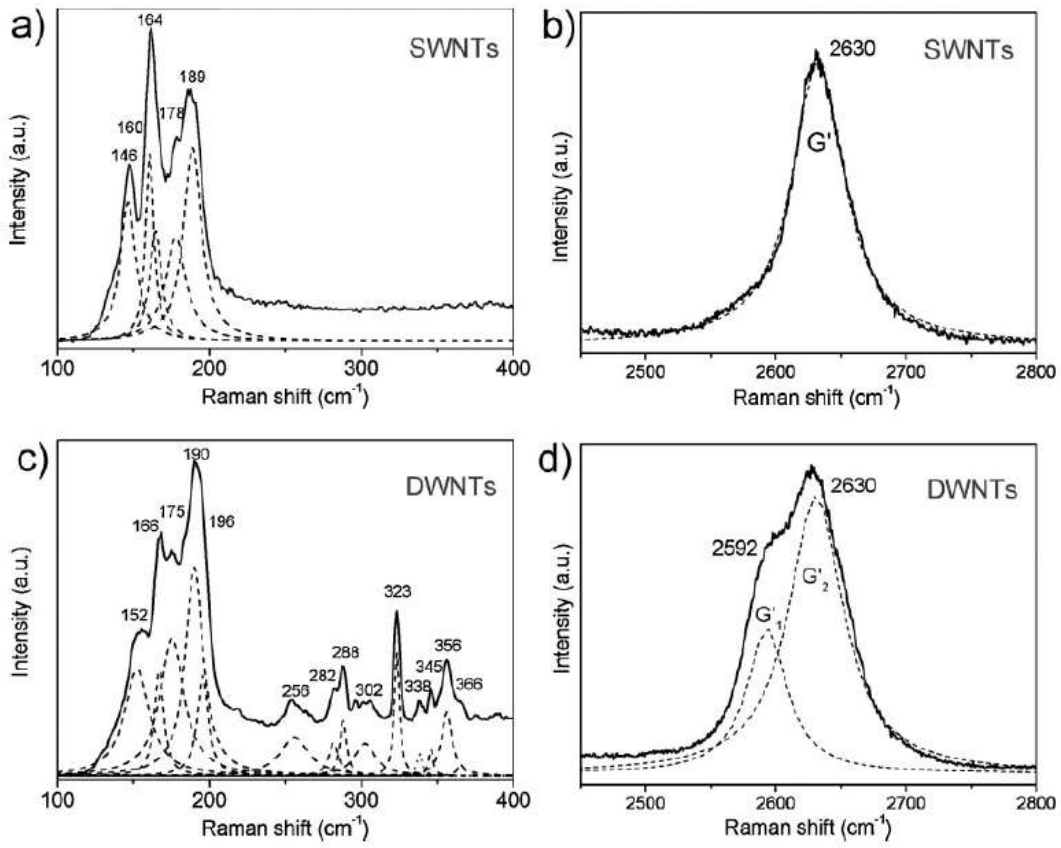

Figure 14: Raman spectra of SWCNTs and DWCNTs obtained using a 633nm HeNe laser. a) Low-frequency region for the SWNTs, showing the RBMs. b) The G' region of the SWCNTs. c) Low-frequency region for the DWNTs, showing the additional RBMs. d) The G' region of the DWNTs, showing splitting of the band (Reprinted from (Cui et al. 2009), with permission from Elsevier)

Cui et al. (Cui et al. 2009) employed Raman Spectroscopy to study the effect of stress transfer in a double-walled carbon nanotube reinforced matrix. DWNTs are the simplest form of MWNTs. In this respect they can be employed to study both the polymer graphene interface as well as the wall to wall interface. In their study Cui et al monitor the stress induced shift of the Raman bands of DWNTs during deformation and employ their findings to predict the behaviour of MWNTs. Cui et al verify the splitting of the G' band when a model composite system is subjected to tension and compression (Figure 14). As the splitting is attributed to slippage of the inner wall of the DWCNT, the authors use the stress-induced shift of the outer and inner wall to predict effective reinforcement in MWCNT reinforced composites. They report poor inter-wall bonding or even that the inner nanotube wall is "virtually unstressed" to conclude that the effective Young's modulus in MWCNT reinforced systems is bound

to be relatively low unless the inter-wall stress transfer is improved, potentially through the introduction of defects, or subsequent treatments such as radiation crosslinking (Peng et al. 2008).

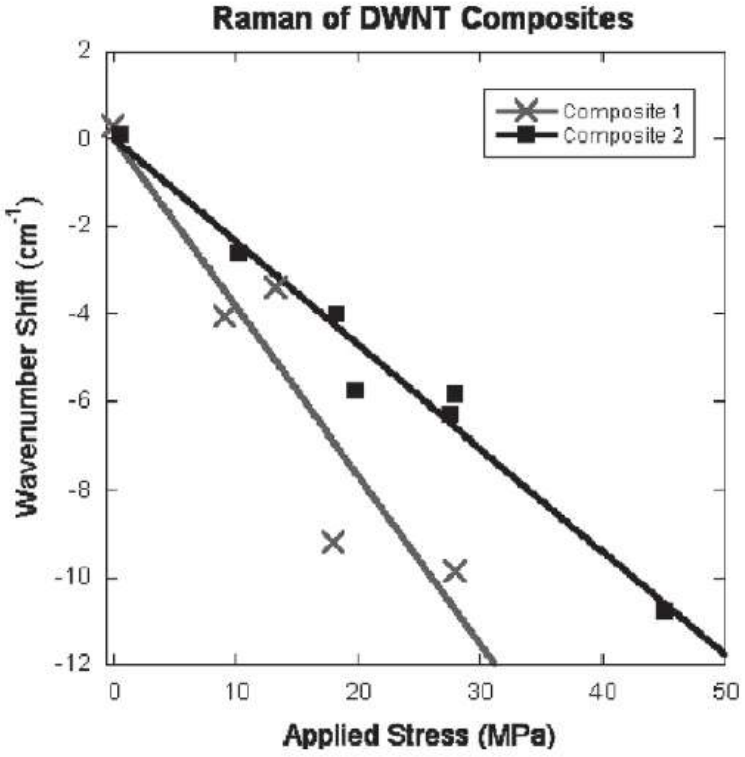

Figure 15: Raman peak shift as a function of applied tensile stress for two nanotube composite samples (Reprinted from (Brownlow et al. 2010), with permission from Elsevier)

Apart from the effect of applied strain on CNT nano-composites, the Raman shift has also been employed to study their residual strains in composites. Hadjiev et al (Hadjiev et al. 2010) employed Raman Microscopy to measure residual strain in CNT reinforced epoxies. They took advantage of the difference in frequencies of the CNT vibrational G^+ mode in the composite compared to that of relaxed CNTs to measure the local residual strains in the composites. They report considerable variation with both CNT functionalization and CNT concentration. More specifically, at room temperature and with the same local concentration of CNTs in the composite, the strains of oxidized and polyamidoamine-functionalized CNTs are found to be 2.5 times higher than that of the composite containing pristine CNTs. According to the authors, the higher residual strain of the composites loaded with functionalized CNTs is indicative of better stress transfer and integration in the epoxy matrix, which was verified by the improved tensile properties measured for the functionalized CNT

composites. Interestingly enough, the residual strain is reported to depend on other parameters than the thermal coefficient mismatch between the CNTs and the epoxy, which in its turn is independent of post processing of the CNTs. However, the authors do not report the effect of post processing on the spectrum of CNTs prior to incorporation into the matrix. Lucas and Young (Lucas,Young 2007a) report on the spectral changes in the RBM and the G' line induced by the thermal stresses in SWCNT reinforced composites. They employ epoxies cured at different temperatures to induce varied thermal stress field in the CNT reinforced polymer. They report that the relative intensities of the RBM vary with curing temperature, and correlate this variation to that induced by far-field strain application, when the composites are loaded in four-point flexure. They also report a red shift of the G' band with increasing curing temperature and employ the measured shift to verify the reported thermal expansion coefficient of the epoxy matrix. Additionally, the effect of strain on RBM is studied using three different excitation wavelengths in order to study the well-known dispersive features of the RBM with applied strain (Lucas,Young 2007b). The authors report variations of between 10% and 200% of the RBM intensities over a range of strain between −0.6% and 0.7% depending on the nanotube diameter and its chirality accompanied by a shift of the G and G′ bands. They attribute these intensity changes to resonance effects and employ tight-binding calculations to predict intensity changes with uniaxial strain.

Comparative studies of the efficiency of CNTs as strain sensors have also been recently published (Sureeyatanapas et al. 2010). Both luminescence and Raman spectroscopy have been employed to monitor the stress build-up on the fibre of a single fibre fragmentation coupon. The authors combine single-walled nanotubes with a silane coating on the surface of samarium doped glass fibres. Thus, local strain could be simultaneously monitored using both techniques, despite the presence of this coating. Good agreement with shear-lag theory can be obtained using both techniques, during the fragmentation of the glass fibre. De la Vega et al combine impedance spectroscopy with Raman spectroscopy to monitor the thermal stress built up during curing (de la Vega et al. 2009) and to simultaneously sense local and global strain in a carbon nanotube reinforced composite (De la Vega et al. 2011). In order to successfully monitor the stress built-up during curing, they correct the apparent Raman shifts with temperature. Although the Raman probing is sensitive enough to temperature and phase changes, there is no observable slope change in the

conductivity of the cured samples reheated up to their ultimate processing temperature. Cured SWCNT epoxy composites above electrical percolation are simultaneously studied and a similar behavior is observed for both the Raman Shift and the electrical conductivity of the nano composite. Both techniques are found to undergo transitions beyond a critical strain level which according to the authors, coincides with the development of residual strain in the matrix, when the composites were subjected to cyclic loading.

Nano-reinforced composites with higher symmetry would include nano-reinforced fibres, which due to manufacturing processes favour alignment along the fibre axis. These nano-reinforced composites would be transversely anisotropic in terms of symmetry. Polarised Raman spectroscopy has been employed to characterize the alignment of the nano-reinforcement along the fibre axis, which would be a measure of the quality of the CNT-reinforced fibres. Chae et al (Chae et al. 2005) study polyacrylonitrile (PAN)/ CNTs composite fibres, spun from solutions in dimethyl acetamide (DMAc), using SWCNTs, DWCNTs, MWCNTs, and vapour grown carbon nano-fibres (VGCNFs). The CNT content in all cases was 5 wt%. In this case, Raman spectroscopy is employed for characterising the fibre morphology rather than the efficiency of the stress transfer or orientation. Chen and Tao (Chen,Tao 2006) report a manufacturing method of polymer nanocomposites with SWNTs by casting a suspension of SWNTs in a solution of thermoplastic polyurethane and tetrahydrofuran. In their case, the nano-reinforced composite is a thin film of well aligned SWCNTs. They achieve very good alignment and improved mechanical properties. Polarized Raman spectroscopy was employed to verify the achieved orientation. The authors attribute this orientation to the macroscopic alignment which results from solvent–polymer interaction induced orientation of soft segment chain during swelling and moisture curing. The study of stress transfer using Raman Spectroscopy in fibre geometries is reported by Lachman et al (Lachman et al. 2009). They report on the strain sensitivity of the G' Raman band of SWCNTs in polyvinyl alcohol-SWCNT composite fibres, with a view to employing such structures as strain or stress sensors when embedded in structural components. They observe higher shifts of the G' Raman band when carboxylic functional groups are present at the nanotube surface and attribute this behaviour to improved interfacial adhesion. According to the authors, this enhancement of the interface increases the efficiency of such structures when used as stress sensors. However, they also report that improvements in

interfacial adhesion do not lead to substantially better mechanical properties of the fibres. They explained this controversy by considering possible degradation of nanotubes during surface functionalisation. Their finding is important in that modification of CNTs with respect to achieving more efficient stress transfer may have adverse effect in other functionalities, such as reinforcement.

Deng et al (Deng et al. 2010) report on the manufacturing of Poly(p-phenylene terephthalamide)/single-walled carbon (PPTA/SWNT) composite fibres with different draw ratios using a dry-jet wet spinning process. The fibres were subsequently monitored using Raman spectroscopy. Raman scattering intensity mapping along the fibre is employed as a measure of the dispersion of the nano-reinforcement. The authors report that the nanotubes improve the polymer orientation in composite fibre with a draw ratio of 2 but degrade the orientation at higher draw ratios, and suggest that the reinforcement is more likely to be due to polymer chain orientation rather than nano-reinforcement. The interface of their studied system is reported to fail at far field strain higher than 0.35%. They also performed cyclic tests to assess the reversible deformation behaviour of the fibre as well as the gradual damage of the interface at high strains. They suggest that the hysteretic behaviour of the fibres in cyclic loading renders them useful in structural damping applications.

Blighe at al (Blighe et al. 2011) measured the mechanical properties of coagulation-spun polymer–nanotube composite fibres with a volume fraction up to ~10%. They employed polarized Raman Spectroscopy to show (i) that orientation increases with drawing, indicating that significant nanotube alignment occurs and (ii) to demonstrate that the nanotube effective modulus also increases with drawing which suggests that the nanotube alignment in the fibres may be further improved. The authors introduce an empirical relationship between Krenchel's nanotube orientation efficiency factor (in other words the experimental deviation from the rule of mixtures) and calculate an orientation parameter via Raman Spectroscopy. They confirm that fibre modulus and fibre strength scales linearly with orientation and proceed to the calculation of the effective interfacial shear strength and critical length (40 MPa and 1250 nm respectively).

An interesting study of the deformation of DWCNT/ epoxy composites employs a lamina configuration. Functionalized mats of DWCNTs are used to manufacture nano-reinforced composites where the distribution of the DWCNTs was practically 2D (Brownlow et al. 2010). The geometry of the structure can be regarded as

transversely isotropic, but in contrast to the fibre geometry, the axis of symmetry is located vertical to the mat plane. The authors employ both FTIR and Raman. The FTIR technique is employed to estimate the average matrix stress, whereas the G' peak shift is employed to monitor the stress build up in the composite. The authors report a large stress-induced shift in the G' peak of 3.7 cm^{-1}/GPa which, compared to the "universal stress sensor" of approximately 5 cm^{-1}/GPa, is remarkably good and probably better than what a random 2D distribution of short reinforcing fibres should exhibit (figure 15). This experimental finding is indicative of the effect of the CNT distribution on the reinforcing ability of the nanophase.

Last but not least, very recent works focus on the interfacial shear stress transfer in model composites where graphene is embedded in a matrix and the Raman probe provides information on the stress built up on the sp^2 sheet. Srivastava et al (Srivastava et al. 2011) employed graphene as a filler and monitored the strain induced shifts of the G band shift of graphene platelets in polydimethyl-siloxane (nanocomposites. In their study, they report large debonding strains of ~7% for graphene in the matrix, and a G band strain sensitivity of~2.4 cm−1 / strain % which, compared to the measured shift of 0.1 cm−1 /% for single-walled carbon nanotube composites, suggests enhanced load-transfer. The surprising observation is that for strains higher than 2% the G line shifted to higher wave numbers reproducibly. The authors attribute this behaviour to the alignment of the polymer chains due to tension which results in lateral compression of the graphene platelets.

Gong et al (Gong et al. 2010) used Raman spectroscopy to monitor the stress transfer on a mechanically cleaved single graphene monolayer embedded in a thin polymer matrix layer. They monitored the G' band shifts for their study. For strains up to 0.4%, the authors report a linear dependence of the G' band. As the stress induced Raman shift exhibits a plateau at this strain level, the authors conclude that no further stress transfer can be sustained by the graphene/ epoxy interface. The stress induced shift is measured to be as high as 60 cm^{-1}/% in the case of unloading of the strained sample. The authors employ the shear-lag model (Cox 1952) and the Kelly Tyson formula (Kelly,Tyson 1965) to calculate interfacial shear strength of 2.3 MPa and 0.3-0.8 MPa respectively which is a magnitude lower than the respective strength of carbon fibre epoxy interfaces. However, they suggest that the low values may be due to the fact that the interrogated graphene layer is shorter than the critical length required to build adequate axial stress.

Concluding, the incorporation of carbon nano-scaled structures in polymer matrices is very promising in providing stress transfer monitoring and stress sensing functionalities in the nano-reinforced composite using Raman Spectroscopy, as has already been performed in the case of carbon fibres. As should be noted the spectral signature and the stress induced shifts of any sp^2 structure is very dependent on the structure itself, the dispersion in the matrix, and the reinforcing symmetry. The uniqueness of the stress dependence of the Raman spectrum of any of these structures is complicating the task of calibrating the stress-induced changes in the Raman spectrum for the nano-reinforced composites. On the other hand, this uniqueness may be paramount in providing specific information about the stress transfer at the nanoscale. This is becoming more prominent as knowledge on the induced spectral changes is accumulating. Additionally, as the maximum value of the force constant should be the same for all sp^2 structures, this may provide a measure of the reinforcing ability of the nanophase as compared with the ultimate translation of the far field stress on the C-C bond.

6.6. Summary

The scope of this work is to provide an overview of the stress induced changes in the Raman spectrum of graphitic structures with a view to elucidating the reinforcing ability of the CNTs in a matrix and assess the stress transfer at the CNT matrix interface. At the same time the research effort towards employing CNTs as stress sensors in composite materials is presented.

To this end, an overview of the Raman Vibrational modes for all graphitic structures is presented starting from graphite fibres, to SWNTs to MWNTs and finally to Single and Multi-layer Graphene. The distinct differences in the Raman spectrum of these structures are highlighted.

Following this, the principle of the stress dependence of the Raman vibrational modes is presented in the general case. The basic principle of the anharmonic oscillator is presented in order to provide the reader an insight on the underlying principle of stress monitoring.

An overview of the induced changes in the Raman Spectrum of Graphite fibres, Nanotubes and Graphene is presented, either via pressure (hydrostatic or not) or direct

stress application. An extensive literature survey is presented to cover all aspects of the changes in different Raman vibrational modes. Direct stress application on graphene has enabled the introduction of a unique stress sensor which characterizes all sp^2 graphitic structures and may characterize the reinforcing ability of the nanophase.

Finally, an extensive review of the Raman stress monitoring of nano-reinforced composites is presented. The review covers aspects relating to the reinforcing ability of the nanophase, the stress-sensing capability, as well as the stress transfer at the graphene/ epoxy interface or even at the interface between the distinct layers in DWCNTs.

6.7. References

Arjyal, B.P., Katerelos, D.G., Filiou, C., Galiotis, C.: Measurement and modeling of stress concentration around a circular notch. Experimental Mechanics **40**(3), 248-255 (2000)

Bahr, J.L., Yang, J., Kosynkin, D.V., Bronikowski, M.J., Smalley, R.E., Tour, J.M.: Functionalization of carbon nanotubes by electrochemical reduction of aryl diazonium salts: A bucky paper electrode. Journal of the American Chemical Society **123**(27), 6536-6542 (2001)

Bandow, S., Hirahara, K., Hiraoka, T., Chen, G., Eklund, P.C., Iijima, S.: Turning Peapods into Double-Walled Carbon Nanotubes. MRS Bulletin **29**(4), 260-264+239 (2004)

Barber, A.H., Zhao, Q., Wagner, H.D., Baillie, C.A.: Characterization of E-glass-polypropylene interfaces using carbon nanotubes as strain sensors. Composites Science and Technology **64**(13-14), 1915-1919 (2004)

Belandria, E., Millot, M., Broto, J.M., Flahaut, E., Rodriguez, F., Valiente, R., Gonzalez, J.: Pressure dependence of Raman modes in double wall carbon nanotubes filled with 1D Tellurium. Carbon **48**(9), 2566-2572 (2010). doi:10.1016/j.carbon.2010.03.036

Benoit, J.M., Buisson, J.P., Chauvet, O., Godon, C., Lefrant, S.: Low-frequency Raman studies of multiwalled carbon nanotubes: Experiments and theory. Physical Review B - Condensed Matter and Materials Physics **66**(7), 734171-734174 (2002)

Blighe, F.M., Young, K., Vilatela, J.J., Windle, A.H., Kinloch, I.A., Deng, L., Young, R.J., Coleman, J.N.: The effect of nanotube content and orientation on the mechanical properties of polymer-nanotube composite fibers: Separating intrinsic reinforcement from orientational effects. Advanced Functional Materials **21**(2), 364-371 (2011)

Bretzlaff, R.S., Wool, R.P.: Frequency shifting and asymmetry in infrared bands of stressed polymers. Macromolecules **16**(12), 1907-1917 (1983)

Brown, S.D.M., Jorio, A., Corio, P., Dresselhaus, M.S., Dresselhaus, G., Saito, R., Kneipp, K.: Origin of the Breit-Wigner-Fano lineshape of the tangential G-band feature of metallic carbon nanotubes. Physical Review B - Condensed Matter and Materials Physics **63**(15), 1554141-1554148 (2001)

Brownlow, S.R., Moravsky, A.P., Kalugin, N.G., Majumdar, B.S.: Probing deformation of double-walled carbon nanotube (DWNT)/epoxy composites using FTIR and Raman techniques. Composites Science and Technology **70**(10), 1460-1468 (2010)

Can, ccedil, ado, L.G., Pimenta, M.A., Saito, R., Jorio, A., Ladeira, L.O., Grueneis, A., Souza-Filho, A.G., Dresselhaus, G., Dresselhaus, M.S.: Stokes and anti-Stokes double resonance Raman scattering in two-dimensional graphite. Physical Review B **66**(3), 035415 (2002)

Cançado, L.G., Pimenta, M.A., Neves, B.R.A., Medeiros-Ribeiro, G., Enoki, T., Kobayashi, Y., Takai, K., Fukui, K.I., Dresselhaus, M.S., Saito, R., Jorio, A.: Anisotropy of the Raman spectra of nanographite ribbons. Physical Review Letters **93**(4), 047403-047401 (2004)

Cançado, L.G., Takai, K., Enoki, T., Endo, M., Kim, Y.A., Mizusaki, H., Speziali, N.L., Jorio, A., Pimenta, M.A.: Measuring the degree of stacking order in graphite by Raman spectroscopy. Carbon **46**(2), 272-275 (2008)

Chae, H.G., Sreekumar, T.V., Uchida, T., Kumar, S.: A comparison of reinforcement efficiency of various types of carbon nanotubes in polyacrylonitrile fiber. Polymer **46**(24), 10925-10935 (2005). doi:10.1016/j.polymer.2005.08.092

Chen, W., Tao, X.: Production and characterization of polymer nanocomposite with aligned single wall carbon nanotubes. Applied Surface Science **252**(10), 3547-3552 (2006). doi:10.1016/j.apsusc.2005.05.028

Chohan, V., Galiotis, C.: Effects of interface, volume fraction and geometry on stress redistribution in polymer composites under tension. Composites Science and Technology **57**(8), 1089-1101 (1997)

Christofilos, D., Arvanitidis, J., Tzampazis, C., Papagelis, K., Takenobu, T., Iwasa, Y., Kataura, H., Lioutas, C., Ves, S., Kourouklis, G.A.: Raman study of metallic carbon nanotubes at elevated pressure. Diamond and Related Materials **15**(4-8), 1075-1079 (2006). doi:10.1016/j.diamond.2005.11.027

Coleman, J.N., Khan, U., Blau, W.J., Gun'ko, Y.K.: Small but strong: A review of the mechanical properties of carbon nanotube-polymer composites. Carbon **44**(9), 1624-1652 (2006)

Colthup, N.B.: Introduction to Infrared and Raman Spectroscopy, Academic Press. Academic Press, London (1975)

Cooper, C.A., Cohen, S.R., Barber, A.H., Wagner, H.D.: Detachment of nanotubes from a polymer matrix. Applied Physics Letters **81**(20), 3873-3875 (2002)

Cooper, C.A., Young, R.J., Halsall, M.: Investigation into the deformation of carbon nanotubes and their composites through the use of Raman spectroscopy. Composites Part A: Applied Science and Manufacturing **32**(3-4), 401-411 (2001)

Cox, H.L.: The elasticity and strength of paper and other fibrous materials. British Journal of Applied Physics **3**(3), 72-79 (1952)

Cronin, S.B., Swan, A.K., Uuml, nl, S., M., Goldberg, B.B., Dresselhaus, M.S., Tinkham, M.: Measuring the Uniaxial Strain of Individual Single-Wall Carbon Nanotubes: Resonance Raman Spectra of Atomic-Force-Microscope Modified Single-Wall Nanotubes. Physical Review Letters **93**(16), 167401 (2004)

Cronin, S.B., Swan, A.K., Uuml, nl, S., M., Goldberg, B.B., Dresselhaus, M.S., Tinkham, M.: Resonant Raman spectroscopy of individual metallic and semiconducting single-wall carbon nanotubes under uniaxial strain. Physical Review B **72**(3), 035425 (2005)

Cui, S., Kinloch, I.A., Young, R.J., Noé, L., Monthioux, M.: The effect of stress transfer within double-walled carbon nanotubes upon their ability to reinforce composites. Advanced Materials **21**(35), 3591-3595 (2009)

De la Vega, A., Kinloch, I.A., Young, R.J., Bauhofer, W., Schulte, K.: Simultaneous global and local strain sensing in SWCNT-epoxy composites by Raman and impedance spectroscopy. Composites Science and Technology **71**(2), 160-166 (2011)

de la Vega, A., Kovacs, J.Z., Bauhofer, W., Schulte, K.: Combined Raman and dielectric spectroscopy on the curing behaviour and stress build up of carbon nanotube-epoxy composites. Composites Science and Technology **69**(10), 1540-1546 (2009)

Del Corro, E., Gonzalez, J., Taravillo, M., Escoffier, W., Baonza, V.G.: Graphite under non-hydrostatic conditions. High Pressure Research **28**(4), 583-586 (2008)

del Corro, E., Taravillo, M., González, J., Baonza, V.G.: Raman characterization of carbon materials under non-hydrostatic conditions. Carbon **49**(3), 973-979 (2011). doi:DOI: 10.1016/j.carbon.2010.09.064

Deng, L., Young, R.J., van der Zwaag, S., Picken, S.: Characterization of the adhesion of single-walled carbon nanotubes in poly(p-phenylene terephthalamide) composite fibres. Polymer **51**(9), 2033-2039 (2010)

Dresselhaus, M.S., Dresselhaus, G.: INTERCALATION COMPOUNDS OF GRAPHITE. Advances in Physics **30**(2), 139-326 (1981)

Dresselhaus, M.S., Dresselhaus, G., Jorio, A.: Raman spectroscopy of carbon nanotubes in 1997 and 2007. Journal of Physical Chemistry C **111**(48), 17887-17893 (2007)

Dresselhaus, M.S., Dresselhaus, G., Saito, R., Jorio, A.: Raman spectroscopy of carbon nanotubes. Physics Reports **409**(2), 47-99 (2005)

Dresselhaus, M.S., Jorio, A., Hofmann, M., Dresselhaus, G., Saito, R.: Perspectives on carbon nanotubes and graphene Raman spectroscopy. Nano Letters **10**(3), 751-758 (2010)

Dunstan, D.J., Ghandour, A.J.: High-pressure studies of carbon nanotubes. High Pressure Research **29**(4), 548-553 (2009)

Evans, K.E., Gibson, A.G.: Prediction of the maximum packing fraction achievable in randomly oriented short-fibre composites. Composites Science and Technology **25**(2), 149-162 (1986)

Everall, N.J., Lumsdon, J., Christopher, D.J.: The effect of laser-induced heating upon the vibrational raman spectra of graphites and carbon fibres. Carbon **29**(2), 133-137 (1991)

Frank, O., Mohr, M., Maultzsch, J., Thomsen, C., Riaz, I., Jalil, R., Novoselov, K.S., Tsoukleri, G., Parthenios, J., Papagelis, K., Kavan, L., Galiotis, C.: Raman 2D-band splitting in graphene: Theory and experiment. ACS Nano **5**(3), 2231-2239 (2011a)

Frank, O., Tsoukleri, G., Parthenios, J., Papagelis, K., Riaz, I., Jalil, R., Novoselov, K.S., Galiotis, C.: Compression behavior of single-layer graphenes. ACS Nano **4**(6), 3131-3138 (2010)

Frank, O., Tsoukleri, G., Riaz, I., Papagelis, K., Parthenios, J., Ferrari, A.C., Geim, A.K., Novoselov, K.S., Galiotis, C.: Development of a universal stress sensor for graphene and carbon fibres. Nature Communications **2**(1) (2011b). doi:10.1038/ncomms1247

10.1021/nn103493g; Huang, M., Yan, H., Heinz, T.F., Hone, J., Probing strain-induced electronic structure change in graphene by Raman spectroscopy (2010) Nano Lett., 10, pp. 4074-4079; Lomax, R., (2007) Statistical Concepts, , Lawrence Erlbaum Associates

Galiotis, C., Batchelder, D.N.: Strain dependencies of the first- and second-order Raman spectra of carbon fibres. (1988)

Galiotis, C., Chohan, V., Paipetis, A., Vlattas, C.: Interfacial measurements and fracture characteristics of single and multi-fiber composites by remote laser Raman microscopy. ASTM Special Technical Publication **1290**, 19-33 (1996)

Galiotis, C., Robinson, I.M., Young, R.J., Smith, B.J.E., Batchelder, D.N.: STRAIN DEPENDENCE OF THE RAMAN FREQUENCIES OF A KEVLAR 49 FIBRE. Polymer communications Guildford **26**(12), 354-355 (1985)

Galiotis, C., Young, R.J., Batchelder, D.N.: A resonance Raman spectroscopic study of the strength of the bonding between an epoxy resin and a polydiacetylene fibre. Journal of Materials Science Letters **2**(6), 263-266 (1983)

Gao, B., Jiang, L., Ling, X., Zhang, J., Liu, Z.: Chirality-dependent Raman frequency variation of single-walled carbon nanotubes under uniaxial strain. Journal of Physical Chemistry C **112**(51), 20123-20125 (2008). doi:10.1021/jp809374j

Gong, L., Kinloch, I.A., Young, R.J., Riaz, I., Jalil, R., Novoselov, K.S.: Interfacial stress transfer in a graphene monolayer nanocomposite. Advanced Materials **22**(24), 2694-2697 (2010)

Gouadec, G., Colomban, P.: Raman Spectroscopy of nanomaterials: How spectra relate to disorder, particle size and mechanical properties. Progress in Crystal Growth and Characterization of Materials **53**(1), 1-56 (2007)

Guo, J.J., Liu, G.H., Wang, X.M., Fujita, T., Xu, B.S., Chen, M.W.: High-pressure Raman spectroscopy of carbon onions and nanocapsules. Applied Physics Letters **95**(5) (2009)

Hadjiev, V.G., Warren, G.L., Sun, L., Davis, D.C., Lagoudas, D.C., Sue, H.J.: Raman microscopy of residual strains in carbon nanotube/epoxy composites. Carbon **48**(6), 1750-1756 (2010)

Hanfland, M., Beister, H., Syassen, K.: Graphite under pressure: Equation of state and first-order Raman modes. Physical Review B **39**(17), 12598 (1989)

Huang, Y., Young, R.J.: Effect of fibre microstructure upon the modulus of PAN- and pitch-based carbon fibres. Carbon **33**(2), 97-107 (1995)

Jorio, A., Dresselhaus, G., Dresselhaus, M.S., Souza, M., Dantas, M.S.S., Pimenta, M.A., Rao, A.M., Saito, R., Liu, C., Cheng, H.M.: Polarized Raman study of single-wall semiconducting carbon nanotubes. Physical Review Letters **85**(12), 2617-2620 (2000)

Jorio, A., Fantini, C., Dantas, M.S.S., Pimenta, M.A., Souza Filho, A.G., Samsonidze, G.G., Brar, V.W., Dresselhaus, G., Dresselhaus, M.S., Swan, A.K., Ünlü, M.S., Goldberg, B.B., Saito, R.: Linewidth of the Raman features of individual single-wall carbon nanotubes. Physical Review B - Condensed Matter and Materials Physics **66**(11), 1154111-1154118 (2002)

Jorio, A., Pimenta, M.A., Souza Filho, A.G., Samsonidze, G.G., Swan, A.K., Uuml, nl, S., M., Goldberg, B.B., Saito, R., Dresselhaus, G., Dresselhaus, M.S.: Resonance Raman Spectra of Carbon Nanotubes by Cross-Polarized Light. Physical Review Letters **90**(10), 107403 (2003)

Jorio, A., Saito, R., Hafner, J.H., Lieber, C.M., Hunter, M., McClure, T., Dresselhaus, G., Dresselhaus, M.S.: Structural (n, m) determination of isolated single-wall carbon nanotubes by resonant Raman scattering. Physical Review Letters **86**(6), 1118-1121 (2001)

Kao, C.C., Young, R.J.: A Raman spectroscopic investigation of heating effects and the deformation behaviour of epoxy/SWNT composites. Composites Science and Technology **64**(15 SPEC. ISS.), 2291-2295 (2004)

Kao, C.C., Young, R.J.: Assessment of interface damage during the deformation of carbon nanotube composites. Journal of Materials Science **45**(6), 1425-1431 (2010)

Katagiri, G., Ishida, H., Ishitani, A.: Raman spectra of graphite edge planes. Carbon **26**(4), 565-571 (1988)

Kataura, H., Kumazawa, Y., Maniwa, Y., Umezu, I., Suzuki, S., Ohtsuka, Y., Achiba, Y.: Optical properties of single-wall carbon nanotubes. Synthetic Metals **103**(1-3), 2555-2558 (1999)

Kelly, A., Tyson, W.R.: Tensile properties of fibre-reinforced metals: Copper/tungsten and copper/molybdenum. Journal of the Mechanics and Physics of Solids **13**(6), 329-338,in321-in322,339-350 (1965)

Kuzmany, H., Pfeiffer, R., Hulman, M., Kramberger, C.: Raman spectroscopy of fullerenes and fullerene-nanotube composites. Philosophical Transactions of the Royal Society A: Mathematical, Physical and Engineering Sciences **362**(1824), 2375-2406 (2004)

Lachman, N., Bartholome, C., Miaudet, P., Maugey, M., Poulin, P., Wagner, H.D.: Raman response of carbon nanotube/PVA fibers under strain. Journal of Physical Chemistry C **113**(12), 4751-4754 (2009). doi:10.1021/jp900355k

Lespade, P., Marchand, A., Couzi, M., Cruege, F.: Caracterisation de materiaux carbones par microspectrometrie Raman. Carbon **22**(4-5), 375-385 (1984). doi:10.1016/0008-6223(84)90009-5

Liu, Z., Zhang, J., Gao, B.: Raman spectroscopy of strained single-walled carbon nanotubes. Chemical Communications(45), 6902-6918 (2009). doi:10.1039/b914588e

Loa, I., Möschel, C., Reich, A., Assenmacher, W., Syassen, K., Jansen, M.: Novel graphitic spheres: Raman spectroscopy at high pressures. Physica Status Solidi (B) Basic Research **223**(1), 293-298 (2001)

Lucas, M., Young, R.J.: Effect of residual stresses upon the Raman radial breathing modes of nanotubes in epoxy composites. Composites Science and Technology **67**(5), 840-843 (2007a)

Lucas, M., Young, R.J.: Unique identification of single-walled carbon nanotubes in composites. Composites Science and Technology **67**(10), 2135-2149 (2007b)

Lucchese, M.M., Stavale, F., Ferreira, E.H.M., Vilani, C., Moutinho, M.V.O., Capaz, R.B., Achete, C.A., Jorio, A.: Quantifying ion-induced defects and Raman relaxation length in graphene. Carbon **48**(5), 1592-1597 (2010). doi:10.1016/j.carbon.2009.12.057

Malard, L.M., Guimar, atilde, es, M.H.D., Mafra, D.L., Mazzoni, M.S.C., Jorio, A.: Group-theory analysis of electrons and phonons in N -layer graphene systems. Physical Review B **79**(12), 125426 (2009a)

Malard, L.M., Pimenta, M.A., Dresselhaus, G., Dresselhaus, M.S.: Raman spectroscopy in graphene. Physics Reports **473**(5-6), 51-87 (2009b)

Marston, C., Gabbitas, B., Adams, J., Nutt, S., Marshall, P., Galiotis, C.: Failure characteristics in carbon/epoxy composite tows. Composites Part A: Applied Science and Manufacturing **27**(12 PART A), 1183-1194 (1996)

Melanitis, N., Galiotis, C.: Compressional behaviour of carbon fibres - Part 1 A Raman spectroscopic study. Journal of Materials Science **25**(12), 5081-5090 (1990)

Melanitis, N., Tetlow, P.L., Galiotis, C.: Characterization of PAN-based carbon fibres with Laser Raman Spectroscopy. Part I Effect of processing variables on Raman band profiles. Journal of Materials Science **31**(4), 851-860 (1996)

Melanitis, N., Tetlow, P.L., Galiotis, C., Smith, S.B.: Compressional behaviour of carbon fibres - Part II Modulus softening. Journal of Materials Science **29**(3), 786-799 (1994)

Milnera, M., Kürti, J., Hulman, M., Kuzmany, H.: Periodic Resonance Excitation and Intertube Interaction from Quasicontinuous Distributed Helicities in Single-Wall Carbon Nanotubes. Physical Review Letters **84**(6), 1324-1327 (2000)

Nemanich, R.J., Lucovsky, G., Solin, S.A.: Infrared active optical vibrations of graphite. Solid State Communications **23**(2), 117-120 (1977)

Paipetis, A., Galiotis, C.: Effect of fibre sizing on the stress transfer efficiency in carbon/epoxy model composites. Composites Part A: Applied Science and Manufacturing **27**(9), 755-767 (1996). doi:Doi: 10.1016/1359-835x(96)00054-1

Paipetis, A., Galiotis, C.: A study of the stress-transfer characteristics in model composites as a function of material processing, fibre sizing and temperature of the environment. Composites Science and Technology **57**(8), 827-838 (1997)

Paipetis, A., Galiotis, C.: Modelling the stress-transfer efficiency of carbon-epoxy interfaces. Proceedings of the Royal Society A: Mathematical, Physical and Engineering Sciences **457**(2011), 1555-1577 (2001)

Paipetis, A., Galiotis, C., Liu, Y.C., Nairn, J.A.: Stress Transfer from the Matrix to the Fibre in a Fragmentation Test: Raman Experiments and Analytical Modeling. Journal of Composite Materials **33**(4), 377-399 (1999)

Papagelis, K., Andrikopoulos, K.S., Arvanitidis, J., Christofilos, D., Galiotis, C., Takenobu, T., Iwasa, Y., Kataura, H., Ves, S., Kourouklis, G.A.: High pressure Raman study of the second-order vibrational modes of single- and double-walled carbon nanotubes. Physica Status Solidi (B) Basic Research **244**(11), 4069-4073 (2007)

Papagelis, K., Arvanitidis, J., Christofilos, D., Souliou, S.M., Galiotis, C., Ves, S., Kourouklis, G.A.: High-pressure Raman study of stacked-cup carbon nanofibers. High Pressure Research **31**(1), 131-135 (2011)

Peng, B., Locascio, M., Zapol, P., Li, S.Y., Mielke, S.L., Schatz, G.C., Espinosa, H.D.: Measurements of near-ultimate strength for multiwalled carbon nanotubes and irradiation-induced crosslinking improvements. Nat. Nanotechnol. **3**(10), 626-631 (2008). doi:10.1038/nnano.2008.211

Pfeiffer, R., Kuzmany, H., Kramberger, C., Schaman, C., Pichler, T., Kataura, H., Achiba, Y., uuml, rti, J., oacute, lyomi, V.: Unusual High Degree of Unperturbed Environment in the Interior of Single-Wall Carbon Nanotubes. Physical Review Letters **90**(22), 225501 (2003)

Pimenta, M.A., Marucci, A., Empedocles, S.A., Bawendi, M.G., Hanlon, E.B., Rao, A.M., Eklund, P.C., Smalley, R.E., Dresselhaus, G., Dresselhaus, M.S.: Raman modes of metallic carbon nanotubes. Physical Review B - Condensed Matter and Materials Physics **58**(24), R16016-R16019 (1998)

Pitkethly, M.J., Doble, J.B.: Characterizing the fibre/matrix interface of carbon fibre-reinforced composites using a single fibre pull-out test. Composites **21**(5), 389-395 (1990). doi:10.1016/0010-4361(90)90436-z

Proctor, J.E., Gregoryanz, E., Novoselov, K.S., Lotya, M., Coleman, J.N., Halsall, M.P.: High-pressure Raman spectroscopy of graphene. Physical Review B - Condensed Matter and Materials Physics **80**(7) (2009)

Puech, P., Nanot, S., Raquet, B., Broto, J.M., Millot, M., Anwar, A.W., Flahaut, E., Bacsa, W.: Comparative Raman spectroscopy of individual and bundled double wall carbon nanotubes. Physica Status Solidi (B) Basic Research **248**(4), 974-979 (2011)

Robinson, I.M., Zakikhani, M., Day, R.J., Young, R.J., Galiotis, C.: Strain dependence of the Raman frequencies for different types of carbon fibres. Journal of Materials Science Letters **6**(10), 1212-1214 (1987)

Schadler, L.S., Giannaris, S.C., Ajayan, P.M.: Load transfer in carbon nanotube epoxy composites. Applied Physics Letters **73**(26), 3842-3844 (1998). doi:10.1063/1.122911

Sengupta, R., Bhattacharya, M., Bandyopadhyay, S., Bhowmick, A.K.: A review on the mechanical and electrical properties of graphite and modified graphite reinforced polymer composites. Progress in Polymer Science (Oxford) **36**(5), 638-670 (2011)

Souza Filho, A.G., Jorio, A., Samsonidze, G.G., Dresselhaus, G., Dresselhaus, M.S., Swan, A.K., Ünlü, M.S., Goldberg, B.B., Saito, R., Hafner, J.H., Lieber, C.M., Pimenta, M.A.: Probing the electronic trigonal warping effect in individual single-wall carbon nanotubes using phonon spectra. Chemical Physics Letters **354**(1-2), 62-68 (2002)

Srivastava, I., Mehta, R.J., Yu, Z.Z., Schadler, L., Koratkar, N.: Raman study of interfacial load transfer in graphene nanocomposites. Applied Physics Letters **98**(6) (2011). doi:10.1063/1.3552685

Sureeyatanapas, P., Hejda, M., Eichhorn, S.J., Young, R.J.: Comparing single-walled carbon nanotubes and samarium oxide as strain sensors for model glass-fibre/epoxy composites. Composites Science and Technology **70**(1), 88-93 (2010)

Tashiro, K., Wu, G., Kobayashi, M.: Quasiharmonic treatment of infrared and Raman vibrational frequency shifts induced by tensile deformation of polymer chains. Journal of Polymer Science, Part B: Polymer Physics **28**(13), 2527-2553 (1990)

Teredesai, P.V., Sood, A.K., Muthu, D.V.S., Sen, R., Govindaraj, A., Rao, C.N.R.: Pressure-induced reversible transformation in single-wall carbon nanotube bundles studied by Raman spectroscopy. Chemical Physics Letters **319**(3-4), 296-302 (2000)

Tuinstra, F., Koenig, J.L.: Characterization of graphite fiber surfaces with Raman spectroscopy. Journal of Composite Materials **4**, 494-499 (1970)

Van Den Heuvel, P.W.J., Peijs, T., Young, R.J.: Failure phenomena in two-dimensional multi-fibre microcomposites: 2. A Raman spectroscopic study of the influence of inter-fibre spacing on stress concentrations. Composites Science and Technology **57**(8), 899-911 (1997)

Venkateswaran, U.D., Brandsen, E.A., Schlecht, U., Rao, A.M., Richter, E., Loa, I., Syassen, K., Eklund, P.C.: High Pressure Studies of the Raman-Active Phonons in Carbon Nanotubes. physica status solidi (b) **223**(1), 225-236 (2001). doi:10.1002/1521-3951(200101)223:1<225::aid-pssb225>3.0.co;2-6

Vidano, R.P., Fischbach, D.B., Willis, L.J., Loehr, T.M.: Observation of Raman band shifting with excitation wavelength for carbons and graphites. Solid State Communications **39**(2), 341-344 (1981)

Vigolo, B., Penicaud, A., Coulon, C., Sauder, C., Pailler, R., Journet, C., Bernier, P., Poulin, P.: Macroscopic fibers and ribbons of oriented carbon nanotubes. Science **290**(5495), 1331-1334 (2000)

Wool, R.P.: INFRARED STUDIES OF DEFORMATION IN SEMICRYSTALLINE POLYMERS. Polymer Engineering and Science **20**(12), 805-815 (1980)

Yallee, R.B., Young, R.J.: Evaluation of interface fracture energy for single-fibre composites. Composites Science and Technology **58**(12), 1907-1916 (1998)

Zhao, Q., Frogley, M.D., Wagner, H.D.: Direction-sensitive strain-mapping with carbon nanotube sensors. Composites Science and Technology **62**(1), 147-150 (2002)

Zhao, Q., Wagner, H.D.: Two-dimensional strain mapping in model fiber-polymer composites using nanotube Raman sensing. Composites Part A: Applied Science and Manufacturing **34**(12), 1219-1225 (2003)